Icarus 308 (2018) 27–41

Contents lists available at ScienceDirect

Icarus

journal homepage: www.elsevier.com/locate/icarus

# The transitional depositional environment and sequence stratigraphy of Chasma Boreale

S.C. Brothers*, G. Kocurek

*The Jackson School of Geosciences, University of Texas, Austin, TX 78712, USA*

ARTICLE INFO

*Article history:*
Received 27 January 2017
Revised 14 August 2017
Accepted 24 August 2017
Available online 22 September 2017

*Keywords:*
Planum Boreum
Chasma Boreale
Cavi unit
Olympia Undae
Hyperboreae Undae
NPLD
Aeolian sequence stratigraphy

ABSTRACT

The depositional system within Chasma Boreale is unique in that it contains active aeolian environments, expressed as dune fields, and active cryosphere environments, present as layered ice deposits, as well as environments that transition between these. This work presents a new analysis of the Chasma Boreale sediment system that creates an interpretative framework addressing: (a) controls on the balance between aeolian and cryospheric processes in the modern depositional system, (b) the stratigraphic architecture of related sedimentary deposits, and (c) processes of sediment accumulation and preservation. Images from Context Camera (CTX; 6 m/pixel) are used to classify and map sedimentary environments, surfaces, and deposits on the reentrant floor, to refine the established geologic map of the reentrant, and to infer the stratigraphic record of the accumulation from Chasma Boreale's depositional system. A spectrum of sedimentary environments occurring between those dominated by aeolian and by cryospheric processes are identified. Through time, the boundaries of these sedimentary environments have shifted, resulting in complex lateral changes in the configuration of sedimentary environments on the reentrant's floor. Vertically, the stratigraphic record is characterized by the punctuation of sandy aeolian deposits by icy surfaces that indicate episodes of ice growth that preserve underlying deposits, resulting in accumulation. Stabilized icy surfaces occur at multiple vertical (temporal) scales and lateral extents, suggesting the influence of both regional climate change due to allogenic forcing, as well as autogenic dynamics within the transitional system. These observations demonstrate that the Chasma Boreale accumulation can be interpreted in an aeolian sequence stratigraphic framework. This work contributes the first detailed description of the processes forming polar aeolian sequences, with an emphasis on the competing and complementary dynamics between aeolian and cryospheric systems.



## 1. Introduction

Refining the geologic history of Planum Boreum (Fig. 1A) has depended upon interpreting the morphologic evolution of Chasma Boreale (Fig. 1) and the unique stratigraphic record exposed in its walls (Holt et al., 2010; Brothers et al., 2015). The modern sedimentary environment on the reentrant floor, which contains both active dunes (e.g. Bourke, 2006; Schatz et al., 2006) and layered ice deposits (Mullins et al., 2006; Tanaka et al., 2008), is equally important. At present, it is the only identified north polar sedimentary environment to host both a robust aeolian system similar to the circumpolar dune fields (Tsoar et al., 1979; Hayward et al., 2007; Ewing et al., 2010) and a cryospheric system forming icy north polar layered deposits (NPLD; reviewed by Byrne, 2009). The coexistence of these end-member environments indicates that the modern Chasma Boreale depositional system represents a transitional sedimentary environment. This work leverages the transitional character of the system to improve understanding of the interplay between aeolian and cryospheric processes and the resulting mixed ice-sand stratigraphic record

Using image analysis, the depositional system is characterized in a way that reflects the relative dominance of aeolian and cryospheric surface processes. This permits a system-scale evaluation of the balance of surface processes and the boundary condition controls upon these. The range of related stratigraphic architectures is evaluated and incorporated into a refinement of the reentrant's existing geologic map (Tanaka et al., 2008; Tanaka and Fortezzo, 2012) and a reconstruction of the system's stratigraphic record. From the synthesis of Chasma Boreale's geologic map with its process-based stratigraphy arises a model of accumulation and preservation for the entire north polar plateau that is tied to modern system dynamics. The scope provided by this integration recasts the accumulations of both Chasma Boreale and the plateau into a sequence stratigraphic framework, which

* Corresponding author. Present address: The National Academies of Sciences, Engineering, and Medicine, Washington, D.C., 20001, USA.
*E-mail address:* schristian@utexas.edu (S.C. Brothers).

https://doi.org/10.1016/j.icarus.2017.08.038
0019-1035/

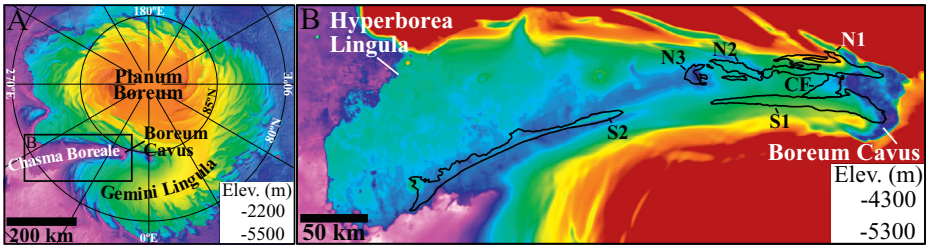


**Fig. 1.** Topography and physiography of the north polar plateau. (A) MOLA topography of Planum Boreum (overlain by a hillshade) annotated with places discussed in the text. (B) Topography of Chasma Boreale. Hyperborea Lingula is the elevated bench of material forming the floor of Chasma Boreale. Boreum Cavus refers to the topographic depression at the head of the reentrant. The boundaries of the six dune fields (northern dune fields N1–N3, central field, CF, and southern fields, S1 and S2) are outlined in black.

couples the stratigraphic architectures with possible allogenic forcing mechanisms. This approach offers a theoretical framework under which polar layered ice and aeolian accumulations can be interpreted together, offering insight not only into recent geologic events influencing sediment systems on both the reentrant floor and on top of the plateau, but also into the accumulation and preservation of the pre-NPLD niveo-aeolian system preserved in the cavi unit (Herkenhoff et al., 2007; Tanaka et al., 2008; Kocurek and Ewing, 2012).

## 2. Geologic context

Chasma Boreale is the 450 km long reentrant that divides Planum Boreum's main dome from its secondary lobe, Gemini Lingula (Fig. 1). Early hypotheses attributed the reentrant's formation to erosional processes ranging from meltwater outflow (Benito et al., 1997; Fishbaugh and Head, 2002) to aeolian incision into pre-existing deposits (Howard, 2000; Warner and Farmer, 2008). More recently, radar sounding has been used to demonstrate that the reentrant formed from accumulation patterns established by the interplay of antecedent topography and katabatic wind flow (Brothers et al., 2015) during early NPLD growth (Holt et al., 2010). The reentrant's stratigraphy is most commonly generalized within the context of Planum Boreum's regional stratigraphy (Fig. 2; Byrne and Murray, 2002; Fishbaugh and Head, 2005; Phillips et al., 2008; Tanaka et al., 2008; Byrne, 2009; Putzig et al., 2009; Tanaka and Fortezzo, 2012).

The basal surface of Chasma Boreale is a bench of material belonging to the Hesperian rupēs unit ($HBb_r$). The bench, Hyperborea Lingula (Fig. 1B), is elevated ~200–300 m above the surrounding plains and is characterized by sandy, even beds (Tanaka et al., 2008). Where exposed, Hyperborea Lingula's surface is heavily cratered and polygonally fractured owing to prolonged exposure to impacts and permafrost processes; local crater counting has yielded an age as old as ~3.5 Ga (Tanaka and Fortezzo, 2012). The bench surface represents an unconformity between $HBb_r$ and subsequent deposits. Elsewhere on the plateau, this unconformity expresses up to a kilometer of erosional relief (Tanaka et al., 2008).

The sandy Middle to Late Amazonian cavi unit ($ABb_c$) overlies the end-rupēs unconformity. While largely eroded from the floor of Chasma Boreale, knobs of $ABb_c$ have persisted in Boreum Cavus, and outcrops line the reentrant's headwall and northern wall (Tanaka and Fortezzo, 2012). These and other outcrops reveal the complicated and diverse stratigraphy within the cavi unit (Byrne and Murray, 2002; Fishbaugh and Head, 2005; Herkenhoff et al., 2007; Tanaka et al., 2008; Kocurek and Ewing, 2012). The unit contains uneven beds of icy and ice-free basaltic sand on the order of meters to tens of meters thick (Tanaka et al., 2008). Cross-stratified intervals are highlighted by the presence of interbedded ice (Herkenhoff et al., 2007). Unit $ABb_c$ also contains

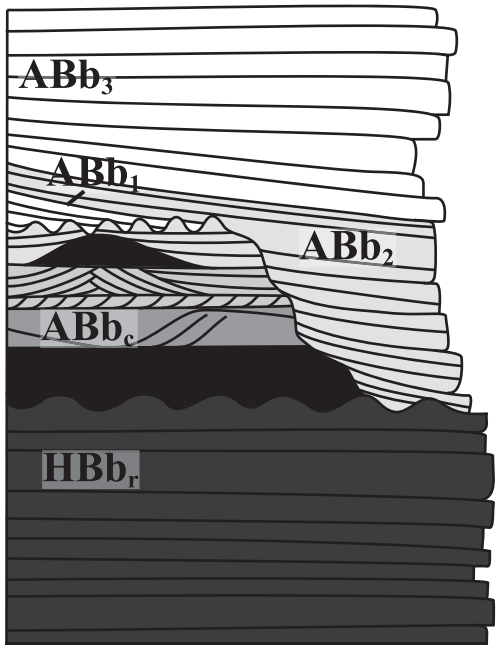


**Fig. 2.** Established stratigraphy of Chasma Boreale, revised from Tanaka et al. (2008). The Hesperian rupēs unit ($HBb_r$) is truncated by an erosional unconformity. Within the reentrant the unconformity is overlain by cavi unit ($ABb_c$) and layered ice mapped as the Planum Boreum 2 unit ($ABb_2$). The presence of the Planum Boreum 1 unit ($ABb_1$) is hypothetical. The Planum Boreum 3 unit ($ABb_3$) overlies $ABb_2$. Units $HBb_r$ and $ABb_c$ comprise the lithostratigraphically defined basal unit (darker shading), which has a higher sand content than overlying water-ice rich layered deposits (lighter shading). Variable shades represent observed variations within and between units (see Section 2).

preserved dune forms, polygonally fractured permafrost surfaces, and layered ice (Kocurek and Ewing, 2012).

Where the cavi unit is absent from the reentrant floor, layered ice deposits overlie the end-rupēs unconformity (Tanaka et al., 2008, Fig. 4A). Collectively, the NPLD are composed of ≥ 95% water ice by volume (Grima et al., 2009). The remaining 5% is dust distributed throughout the ice column. The inclusion of dust is thought to cause the deposits' characteristic layering, although it remains uncertain how the dust is distributed volumetrically (Nunes and Phillips, 2006), and, as a result how the composition relates to optical and mechanical layers (Fishbaugh et al., 2010). Layer formation is commonly attributed to orbitally-forced climate change (Toon et al., 1980; Laskar et al., 2004; Milkovich and Head, 2005; Hvidberg et al., 2012; Becerra et al., 2016). It is generally thought that the growth of the modern ice sheet is tied to a decrease in the planet's obliquity at ~5–4 Ma (Laskar et al., 2002; Levrard et al., 2007).

The NPLD are divided into Planum Boreum units 1 through 3 ($ABb_{1\text{-}3}$; Tanaka and Fortezzo, 2012). These divisions are based

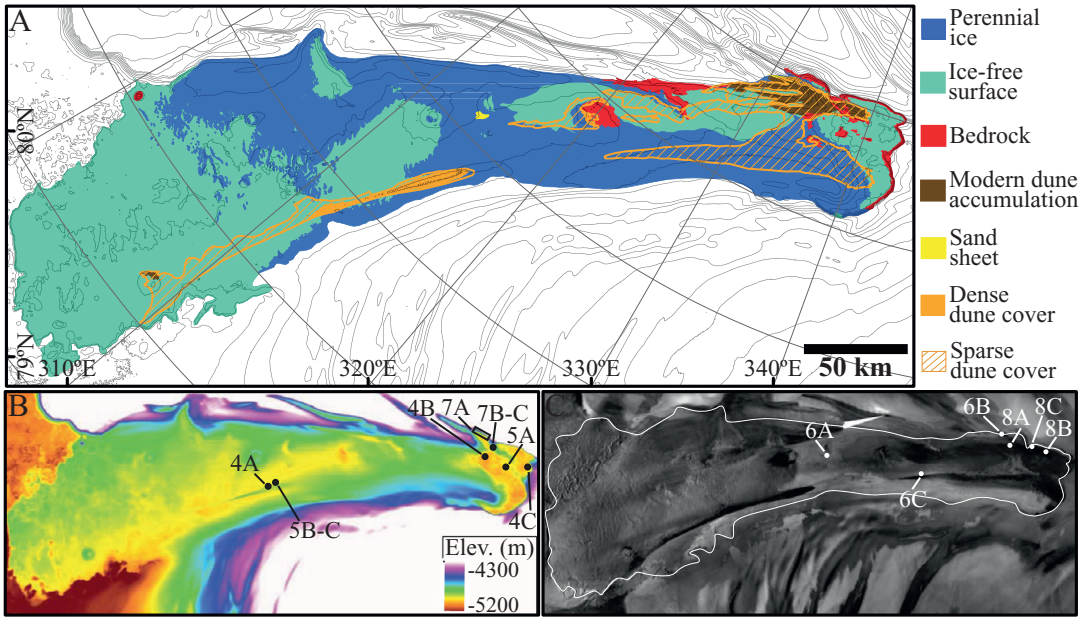


**Fig. 3.** Surface classification of Chasma Boreale. (A) Map of surface types in Chasma Boreale (see Section 4.1). 100 m MOLA contours show background topography. (B) MOLA topography of Chasma Boreale. Locations of Figs. 4, 5, and 7 are shown by labeled black circles. (C) THEMIS-IR Daytime Global Mosaic 100mv12 context for Chasma Boreale. The boundary of Chasma Boreale and Hyperborea Lingula is outlined in white. Mosaic generated by the THEMIS team at ASU (Edwards et al., 2011) and accessed from the USGS Planetary GIS Web Server. Resolution is 115 m/pixel. Locations of Figs. 6 and 8 are given by the labeled white circles.

upon the presence of unconformities (Tanaka et al., 2008) as well as perceived differences in the bulk volume of dust (Tanaka et al., 2008). The lowermost NPLD unit, Planum Boreum 1 ($ABb_1$; Tanaka and Fortezzo, 2012), is not visible on the floor of Chasma Boreale; its presence in the reentrant has been hypothesized owing to the thickness of the accumulation (Tanaka et al., 2008). Crater dating of $ABb_1$ exposures elsewhere indicates an age of $\sim 3.6 \pm 2.5$ Ma (Tanaka and Fortezzo, 2012). The Planum Boreum 2 unit ($ABb_2$) overlies $ABb_1$. Unit $ABb_2$ has been interpreted as comparatively more sediment-rich than other layered ice units. Rodriguez et al. (2007) suggested that $ABb_2$ originated as a discontinuous sand sheet derived from regional erosion of underlying water ice deposits. Within Chasma Boreale, unit $ABb_2$ is exposed in the northern part of the reentrant near Boreum Cavus (Tanaka and Fortezzo, 2012). As mapped by Tanaka and Fortezzo (2012), the reentrant's surface ice deposits belong to the Planum Boreum 3 unit ($ABb_3$). Unit $ABb_3$ includes the most modern layered ice on the plateau.

While the stratigraphy of Planum Boreum and, more locally, Chasma Boreale are well established, the modern depositional system on the reentrant floor is poorly characterized. The active aeolian system is composed of dune fields (Fig. 1B) that are part of Hyperboreae Undae (Tanaka et al., 2008) and are best known for the presence of unusual dune morphologies (e.g., Bourke, 2006; Parteli et al., 2014) indicative of evolution in stabilizing, icy conditions (Schatz et al., 2006; Herrmann et al., 2008; Mullins et al., 2006). An active cryospheric (ice) system is also present on the reentrant floor. This is characterized by permafrost features, such as polygonal fracturing, and perennial NPLD (Tanaka et al., 2008). Although it has been noted that the cyrospheric processes actively modify dune processes in Chasma Boreale (Mullins et al., 2006), this work contributes the first detailed description of competing and complementary dynamics between the modern aeolian and cryospheric systems.

## 3. Methods

The foundation of this work is a classification of sedimentary environments, surfaces, and deposits conducted using 6 m/pixel images from Context Camera (CTX; Malin et al., 2007). CTX images were restricted to those acquired between $L_s$ 90, the beginning of northern summer, and $L_s$ 165, the approximate time at which autumnal clouds begin to obscure the surface. This time range minimized the presence of annual surface frost so that perennial ice deposits could be distinguished. Repeat images from 2006–2014 allowed surface expression consistency to be analyzed. Deposits and surface types were distinguished by apparent albedo (relative brightness within the image being studied), apparent composition, and geomorphic expression. Apparent composition (lithic sediment vs. ice vs. mixture) and geomorphic expression are qualitative characteristics that encompass surface texture (e.g., mottled vs. smooth) and sedimentary structures (e.g., layering or cross-stratification). Where available, High Resolution Imaging Science Experiment (HiRISE; McEwen et al., 2007) observations supplemented surface analysis and classification. Image co-registration and digitization of surface types and unit boundaries were conducted in ESRI'S ArcMAP 10.

The resulting map of sedimentary environments and geologic units permitted stratigraphic cross-sections to be built. Transect topography was from Mars Orbiter Laser Altimeter (MOLA) Experiment Gridded Data Records (MEGDR; Smith et al., 2003). These data have a horizontal resolution of 115 m/pixel (Smith et al., 2003) and a vertical accuracy of approximately 1 m (Smith et al., 2001). Surface geology and near-surface stratigraphy are direct derivatives of the geologic map, with the addition of accumulation estimates (see Section 4.3). Stratigraphy that could not be directly observed was inferred from local contextual evidence (e.g., topographic trends, presence or absence of specific units) and regional stratigraphic norms. Transects were chosen to highlight the diversity of geologic successions within the reentrant.

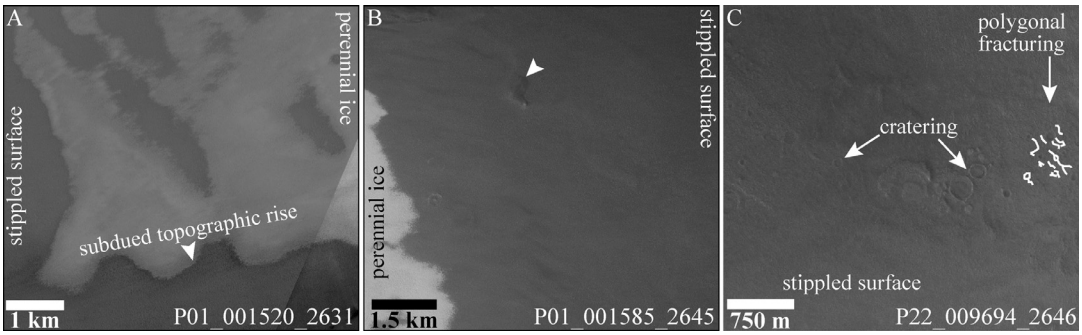


**Fig. 4.** Expressions of surfaces free of perennial ice deposits ("ice-free"). (A) Adjacent to dune field S2 (Fig. 1B), the surface of Hyperborea Lingula is covered by a stippled, intermediate-albedo surface (here overlain by patchy perennial ice) that subdues topographic variations. (B) The stippled surface in Boreum Cavus. A layered outcrop (white arrow) emerges from and is embayed by the stippled surface. Perennial ice deposits initiate on the left-hand side of the frame. (C) Polygonal fracturing (e.g., white lines) and cratering indicate the $HBb_r$ surface. Note the buildup of stippled deposit along the top and bottom of the frame. Image locations are given in Fig. 3B.

## 4. Results

### 4.1. Surface classification

Seven surface types were identified and mapped on the floor of Chasma Boreale (Fig. 3A). The most common surfaces are free of perennial surface ice ("ice-free"; Fig. 3A). Ice-free surfaces cover 17,202 km$^2$ of the reentrant floor and dominate along the reentrant's northern wall, in Boreum Cavus, and on the terminus of Hyperborea Lingula (Fig. 3A). Ice-free surfaces are unified by an intermediate albedo between the dark of dune sands and bright white of layered ice, but exhibit two expressions. Most commonly, Hyperborea Lingula is mantled by a topography-smoothing surface that appears stippled at CTX resolution (Fig. 4A and B). Topographic variations are subdued (Fig. 4A), and positive relief features emerge from beneath the stippled surface (white arrow, Fig. 4B). In places, patchy (Fig. 4A) or thin (Fig. 4B) perennial ice deposits build on top of the stippled surface. Where not mantled the surface of Hyperborea Lingula is characterized by polygonal fracturing and cratering (Fig. 4C). Note that subsurface and/or pore-filling ice is present in the ice-free surfaces, as evidenced by the permafrost structures, but in these locations high albedo ice deposits are not stable at the surface in midsummer.

Perennial surface ice deposits cover 12,281 km$^2$. Thin, patchy ice deposits (e.g., Fig. 4A) are associated with the margins of thicker deposits that are smooth-surfaced and layered (Fig. 5A). Thicker deposits may express evidence for active erosion and precipitation with small changes visible from year to year; layers are particularly prominent where extensive erosion has occurred (Fig. 5B and C). Layered ice may contain high-albedo, icy yardangs (Fig. 5B and C) and low albedo, sandy yardangs (Fig. 6A and C). Large swaths of perennial surface ice also have undulating surface topography with intermittent, exposed low albedo patches (Fig. 6B and C). Accumulations of perennial surface ice occur dominantly along the reentrant's southeastern and northwestern walls; surface ice bridges the central axis of the chasma and connects the wall deposits midway along the reentrant (Fig. 3A).

Bedrock exposures in Chasma Boreale are limited to 679 km$^2$. Bedrock is defined as outcrops of $ABb_c$ (common along the headscarp of Boreum Cavus and intermittently along the reentrant's northern wall (Fig. 3A)), knobs of $ABb_c$ (Figs. 4B, 5A), and windows into the underlying $HBb_r$. Outcrops are layered (Fig. 5A) or cross-stratified (Fig. 7). While steeper exposures are lithified (Fig. 7A), less steep exposures may be poorly consolidated (Fig. 7B) and prone to re-working.

The accumulations of modern dunes cover approximately 461 km$^2$ of the reentrant floor. Modern dune accumulations are recognized where the surface is characterized by sediment deposits expressing arcuate geometries suggestive of plan-view dune lee face morphologies (Fig. 8). Arcuate ridges may form continuous trails with modern dunes of similar geometry, although this is not always the case (Fig. 8A). Some deposits contain a single identifiable set of cross-strata (white arrows, Fig. 8A) whereas in others, multiple sets are discernable (Fig. 8B and C).

Sand sheets and dunes constitute sediment in transport. Sand sheets are identified as areas where low albedo sand sits on a higher albedo surface but lacks sufficient topography to define dunes, or dune definition is obscured by the low contrast surface (Fig. 6B). The area of sand sheets is minor (12 km$^2$) and peripheral to the dune fields (Fig. 3A). Most commonly, dunes occur in spatial densities low enough to map the type of surface upon which they

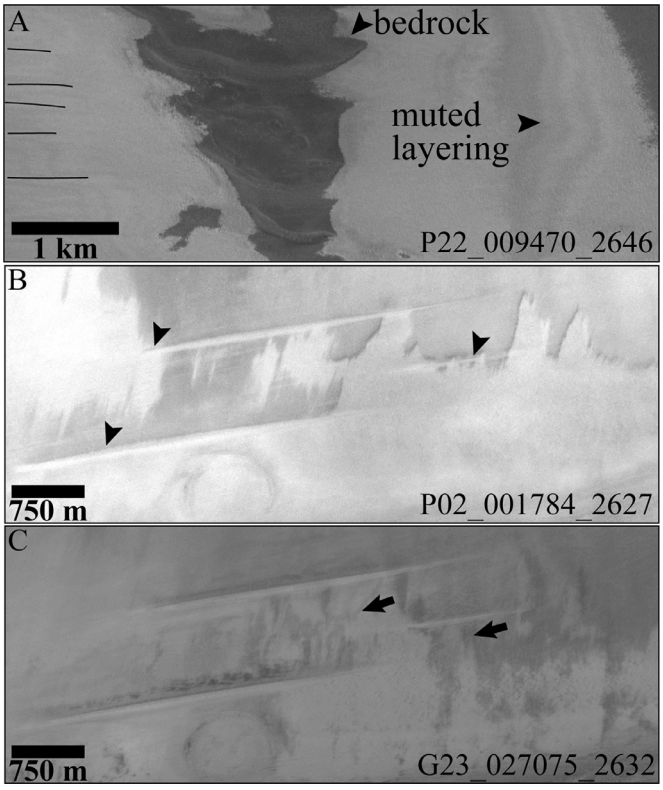


**Fig. 5.** Expressions of perennial surface ice. (A) Layered ice deposits initiating on the stippled surface in Boreum Cavus. Possible erosional grooves (annotated by thin black lines) are visible on the ice surface. (B) Yardangs (black arrows) being exhumed from layered ice. Image acquired in 2006. (C) The same yardangs imaged six years later (2012). Minor changes (black arrows) in ice layers suggest active removal and precipitation. Image locations are given in Fig. 3B.

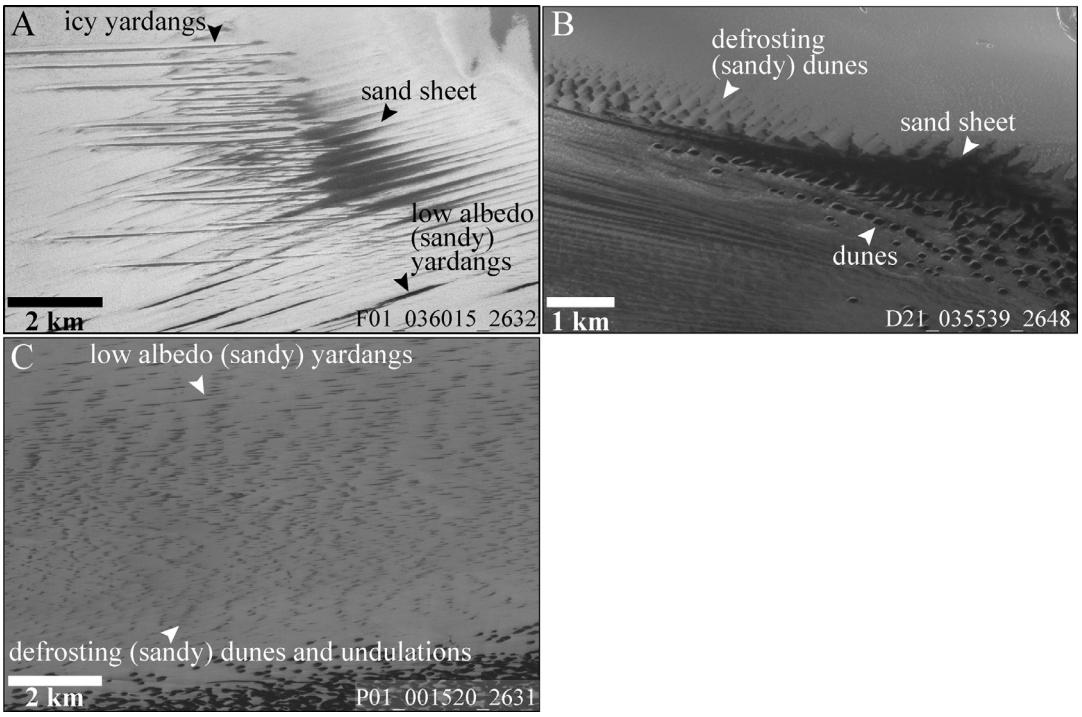


**Fig. 6.** Expressions of sand sheets and ice-covered dunes. (A) Lineated sand sheet. Lineations are parallel to local low albedo yardangs but form oblique to icy yardangs. Sand appears to accumulate around the icy yardangs. (B) A sand sheet on the margin of field N1 (Fig. 1B) transitions southward into dunes and northward into ice deposits from which dunes are emerging. (C) Between the northern and southern dune fields, low albedo transverse and longitudinal features (interpreted as bedforms) are emerging from beneath undulating ice deposits. Figure locations are given in Fig. 3C.

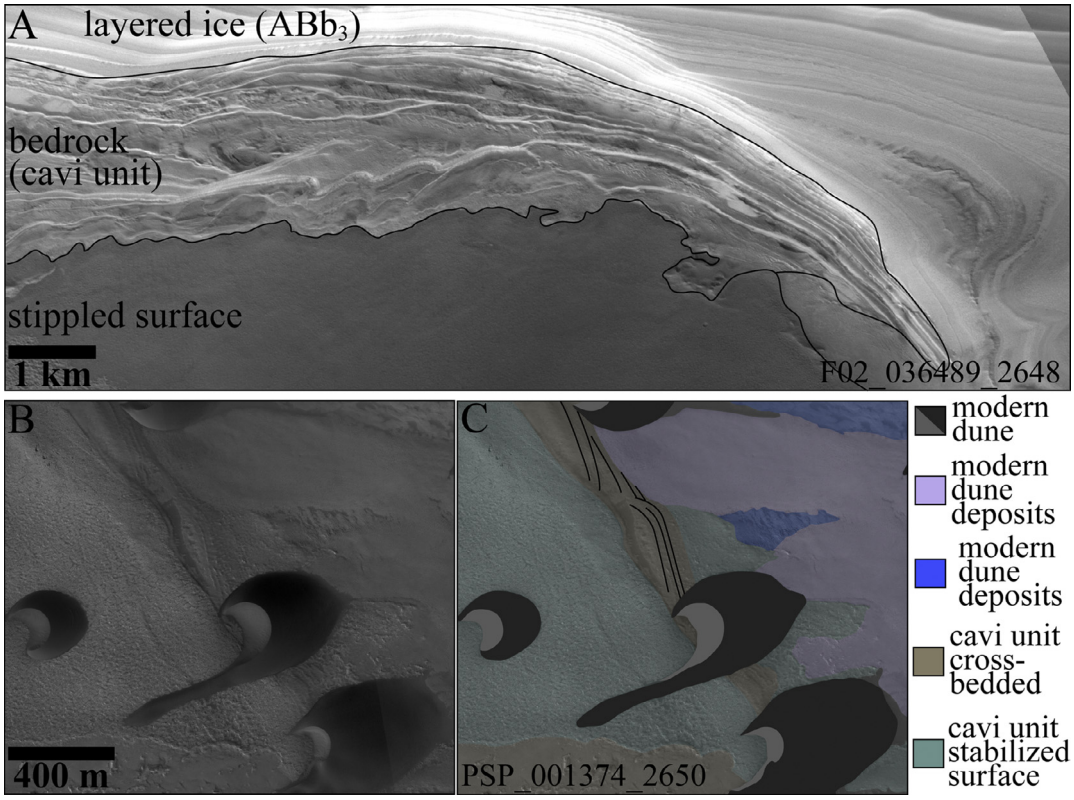


**Fig. 7.** Examples of bedrock exposures. (A) Unevenly bedded and cross-stratified cavi unit exposures line the headwall of Boreum Cavus and crop out along the reentrant's northern wall (Fig. 3A). (B) Dune field N1 is built on top of a low-angle exposure of cavi unit. (C) Same image as (B), with stratigraphic interpretations including stabilized and loosely consolidated cavi unit surfaces and two expressions of modern dune accumulation. Figure locations are given in Fig. 3B.

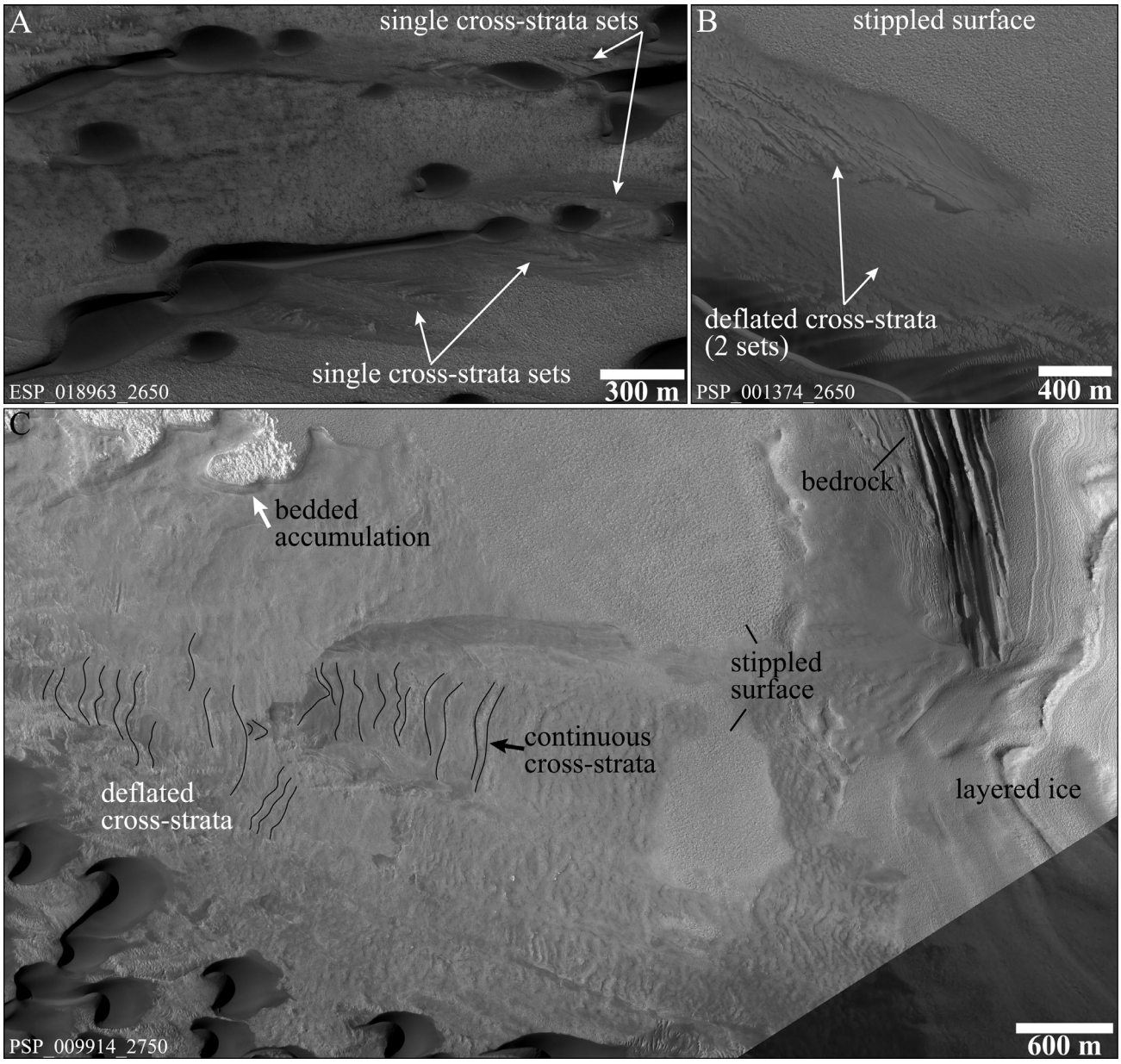


**Fig. 8.** Examples of modern dune accumulations that are cross-stratified in plan-view. (A) Thin accumulations of single cross-strata sets. In places, cross-strata reflect the geometry of the dune downwind (upper white arrows). Cross-strata may also exist without a clear candidate dune (lower white arrows). (B) Thicker accumulations retain discordant cross-strata geometries that suggest the accumulation of multiple dunes. (C) Bedded accumulation (white arrow) capped by a ridged surface. Ridges are reminiscent of cross-strata geometries. Figure locations are given in Fig. 3C. Fig. 13A centers on the bedded accumulation indicated by the white arrow in (C).

rest. In these areas the dune cover is classified as "sparse" and overlaid on the subjacent surface type; sparse dune cover occurs over an area of 3832 km$^2$. Where the underlying surface type could not be determined because of the spatial density of dunes, however, the dune cover is classified as "dense" (246 km$^2$; Fig. 3A).

### 4.2. Geologic map

The surface classification of Chasma Boreale (Fig. 3A) can be integrated into the existing stratigraphic framework of Tanaka and Fortezzo (2012) to create a revised, higher resolution geologic map of the reentrant (Fig. 9A). The fields of modern dunes and associated sand sheets constitute the modern sediment system. As presented in Section 4.1, modern dune accumulations are cross-stratified in plan-view; these form the youngest stratigraphic unit within the reentrant and are expressed locally where conditions have favored dune accumulation. Strata originating from the Hyperboreae Undae dunes are herein designated as stratigraphic unit Planum Boreum Hyperboreae Undae ($ABb_{HU}$, Fig 9A).

Perennial surface ice deposits fall within the Planum Boreum 3 unit ($ABb_3$, Fig. 9A). As described in Section 4.1, Chasma Boreale's $ABb_3$ unit exhibits classical layering as well as the surface expressions of subsurface bedforms. These include fields of yardangs that are interbedded with the ice (e.g., Figs. 5B and C, 6A), low albedo yardangs just below the ice surface and emerging from it (Fig. 6A and C), and similar low albedo ridges reminiscent of transverse bedforms and also emerging from the ice (Fig. 6B and C). The visible extents of these three expressions have been mapped (Fig. 9A). Fields of icy yardangs (icy $ABb_3$ yardangs, Fig. 9A) are exposed between the southern dune fields and extend northward to approximately the central axis of the reentrant. The field of low albedo yardangs (sandy $ABb_3$ yardangs, Fig. 9A) begins north of the icy

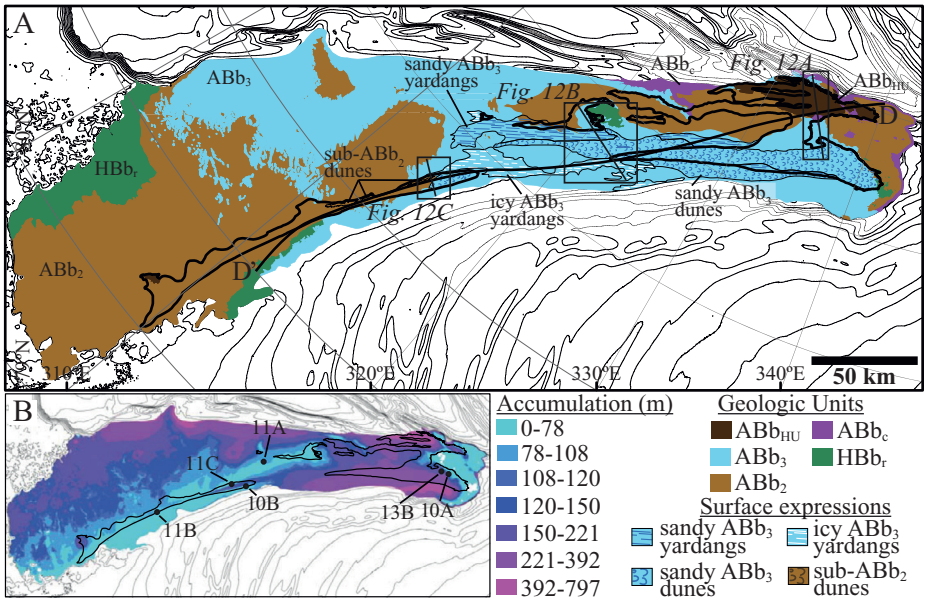


**Fig. 9.** Geologic map of Chasma Boreale, revised from Tanaka and Fortezzo (2012). (A) Stratigraphic units and surface expressions of buried bedforms on the floor of Chasma Boreale. Visible stratigraphic units include the rupēs unit ($HBb_r$), cavi unit ($ABb_c$), Planum Boreum units 2 ($ABb_2$) and 3 ($ABb_3$), and modern dune accumulations ($ABb_{HU}$). Icy yardangs (white lines), dunes exposed by receding perennial ice (blue crescents), and low albedo yardangs interpreted as defrosting linear dunes (blue lines) are superimposed on geologic units. Areas of active sand transport (dune fields and sand sheets) are outlined with heavy black lines. Locations for Fig. 12 are given. Transect D-D' is the location of Fig. 14. 100 m MOLA contours show background topography. (B) Meters of accumulation on the floor of Chasma Boreale, assuming a flat Hyperborea Lingula bench at the elevation of −5025 m. White areas show negative accumulation (erosion) with respect to the chosen bench elevation. Locations for Figs. 10, 11, and 13B are given by the labeled black circles. (For interpretation of the references to color in this figure legend, the reader is referred to the web version of this article.).

yardangs and extends eastward parallel to the northern perennial ice line. Icy and sandy $ABb_3$ yardangs also occur along the southern margin of dune field S1 (Figs. 1, 9A). Along the central axis of the reentrant between the sandy $ABb_3$ and icy $ABb_3$ yardang fields is a field of low albedo ridges emerging from the ice (sandy $ABb_3$ dunes, Fig. 9A). This field is continuous with the boundaries of modern dune field S1, and cross-strata of the sandy $ABb_3$ dunes are visible in scour pits (e.g., Fig. 10A) across the extent of the southern dune field. Bedforms emerging from the $ABb_3$ ice are also present along the windward, icy margin of dune field S2 (Figs. 9A, 10B), as well as north of the northern dune field N1 (Fig. 6B).

Underlying $ABb_3$ and exposed where perennial surface ice is absent is the stippled unit (Fig. 4). Areas of the reentrant where the stippled unit has been identified correspond with few exceptions (see below) to areas mapped by Tanaka and Fortezzo (2012) as the ice-depleted surface of the Planum Boreum 2 unit ($ABb_2$; Fig. 9A). In Boreum Cavus $ABb_2$ is differentiable from the underlying rupēs unit ($HBb_r$, Fig. 9A) surface by the absence of polygonal fractures and extensive cratering at CTX resolution (e.g., Fig. 4B and C). Knobs of $ABb_c$ ($ABb_c$, Fig. 9A) are embayed by the stippled unit (Fig. 4B) and also emerge from and are embayed by $ABb_3$ ice deposits (Fig. 5A). The interpretation of an isolated $HBb_r$ window in the central part of the reentrant (within the context box of Fig. 12B in Fig. 9A) is uncertain due to low image contrast, however, the window's extremely low elevation is more consistent with the $HBb_r$ bench than with $ABb_c$ outcrops and knobs elsewhere in the reentrant (Fig. 3A and B).

Whereas established maps (Tanaka and Fortezzo, 2012) have attributed the surface of the southwestern end of Hyperborea Lingula entirely to $HBb_r$, this is unlikely given pervasive subdued topography beneath the stippled surface (Fig. 11A and C), crater infilling (e.g., Fig. 11A), and a clear contact between the stippled surface and the heavily cratered $HBb_r$ surface (Fig. 11B). The $ABb_2$/$HBb_r$ contact along the southern margin of dune field S2 confirms that younger deposits overlie the older bench surface in this area (Fig. 11B). Crater infilling to the north of the field (Fig. 11A) indicates that locally there may exist a thick accumulation between $HBb_r$ and the modern surface. Along the northern margin of dune field S2, the surface of $ABb_2$ expresses subdued topographic undulations strongly suggestive of dune morphologies (Fig. 11C). No contacts are visible between where the $ABb_2$ surface emerges from beneath local perennial ice deposits and the expression of dunes (Fig. 11C), indicating the dunes underlie the $ABb_2$ surface. These dunes have been mapped as sub-$ABb_2$ dunes (Fig. 9A).

Assuming a flat Hyperborea Lingula bench and an elevation of −5025 m, accumulation on the floor of Chasma Boreale ranges between 0 m and ~800 m (Fig. 9B). Mean accumulation is 155 m with a standard deviation of 95 m. The highest values correspond to locations on the margins of the reentrant where modern layered ice is continuous with deposits on the plateau (Fig. 9). Much more commonly, however, accumulation ranges between 10 s of meters, where the exposed $ABb_2$ surface directly overlies $HBb_r$, to ~400 m in parts of the reentrant characterized by the accumulation of units $ABb_2$ and $ABb_3$.

### 4.3. Stratigraphy derived from the geologic map

Key stratigraphic sections derived from the geologic map (Fig. 12) illustrate the vertical and lateral changes that characterize the Chasma Boreale depositional system. Across the eastern end of the reentrant (Fig. 12A), the accumulation has built upon $ABb_c$ topography. Exposure of $ABb_c$ at the modern surface (Fig. 9A) and the isolated nature of these outcrops (Fig. 12A) indicate that, where present in the reentrant, the surface of $ABb_c$ is erosional. Beneath more recent accumulations, outcrops may be connected or disconnected, and additional topographic relief on the $ABb_c$ surface might be present (e.g., at 10 km, which underlies a local topographic high; Fig. 12A-A'). Where $ABb_c$ is not present, the accumulation rests unconformably on the $HBb_r$ surface. Although topographic relief on this surface is documented (e.g., the topographic low of Boreum Cavus, Fig. 3B), for simplicity, the $HBb_r$ surface is portrayed as approximately flat (Fig. 12A-A').

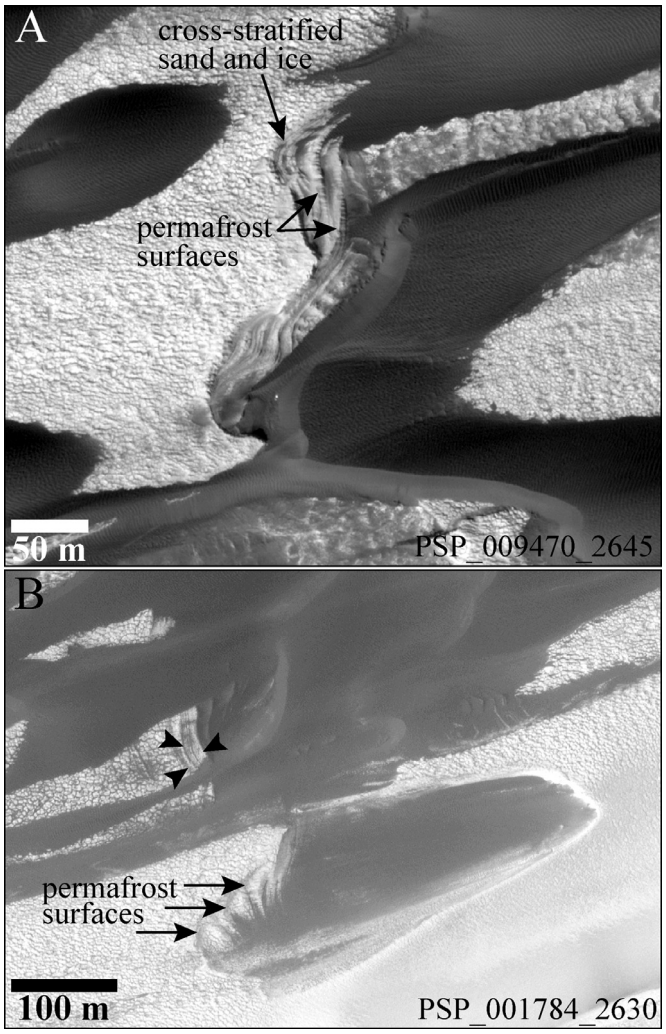


**Fig. 10.** Evidence for cross-stratified ice and sand below dune fields S1 and S2. (A) Modern dunes have scoured into the substrate of field S1, revealing intervals of cross-stratified ice and sand punctuated by horizontal permafrost surfaces. (B) Similar dune imprints on the margins of field S2. Stabilizing permafrost surfaces are denoted by black arrows. Locations are given in Fig. 9B.

Extrapolating from the juxtaposition of geologic units on the surface and from MOLA topography, erosional relief on the $HBb_r$ and $ABb_c$ surfaces has created as much as 100 m of antecedent bedrock topography in the eastern end of the reentrant (Fig. 12A-A'). While remnants of this relief still exist on the surface (e.g., between 20 and 30 km, Fig. 12A-A'), much of it has been infilled by subsequent accumulation. The presence of layered ice unit $ABb_1$ in the reentrant is conjectural (Section 2), and, if present, it is entirely buried beneath later deposits. Planum Boreum 2 unit ($ABb_2$) underlies the accumulation of $ABb_{HU}$ and $ABb_3$ (Fig. 12A). While entirely concealed beneath $ABb_{HU}$ along the transect, $ABb_2$ is visible in patches beneath $ABb_3$ (Fig. 12A, A-A'), indicating that $ABb_2$ closely underlies the surface in places and that the thickness of overlying deposits is variable.

Units $ABb_{HU}$ and $ABb_3$ constitute the most recent accumulations in the eastern end of the reentrant. Documented accumulations of $ABb_{HU}$ consist of as little as a single set of cross-strata (Fig. 8A) to as many as five or six intervals bound by horizontal surfaces (bedded accumulation, Fig. 8C; Fig. 13A, C). The modern surface exhibits evidence for multiple sets of deflated cross-strata; this suggests that intervals are comprised of the accumulation of multiple dunes and are bound by bypass or deflation surfaces similar to the modern surface (Fig. 8C, Inset 1 in Fig. 12A-A'). The thickness of the $ABb_{HU}$ accumulation can be estimated where multiple intervals are present. Upwind of field N1, the $ABb_{HU}$ accumulation consists of nominally two sets of cross-strata (Fig. 8B), which yield approximately 8 m of accumulation. The more extensive bedded deposit downwind of these demonstrates, conservatively, ~20–30 m of accumulation for 5–6 intervals (Figs. 8C, 12A-A', 13A, C).

A similar stratigraphy is revealed in the scour pits of unit $ABb_3$ where it interbeds with sandy dunes in the southern end of the transect (Fig. 10A, Inset 2 in Fig. 12A-A', 13B, D). The walls of scour pits are stepped with recessed intervals of sandy and icy cross-strata punctuated by resistant permafrost surfaces; between 3 and 5 intervals are consistently present in the scour pits (Figs. 10A, 13B, D). Scour depth of dune imprints ranges up to ~20 m (calculated upwind of dune field S2), indicating that the accumulation of $ABb_3$ where it has interbedded with sand dunes and been reworked is comparable to scales of accumulation in the ice-free dunes fields.

A transect across the layered ice bridging the northern and southern wall deposits (Fig. 12B) highlights a different character of the Chasma Boreale accumulation. The $HBb_r$ surface is still interpreted as approximately flat, although the proximity of the northern end of the transect to a window into $HBb_r$ (Fig. 12B) suggests it may locally be at a lower elevation (Fig. 12B-B'). The lack of nearby $ABb_c$ outcrops (Fig. 9A) suggests the absence of cavi unit beneath the transect. Again, the presence of $ABb_1$ layered ice is conjectural; increasing surface elevation to the south suggests growth of ice deposits in that direction and indicates an accumulation of anywhere from less than 50 m to as much as 350 m (Fig. 12B-B'). Unit $ABb_2$ is present in the northern end of the transect (Fig. 12B) and is interpreted to underlie unit $ABb_3$, although scour into $ABb_2$ is likely to have generated the local topographic low at ~5 km (Fig. 12B-B') that is now infilled by $ABb_3$ ice.

Based upon estimates of accumulation for re-worked $ABb_3$ deposits beneath dune field S2 (Fig. 12A-A'), the simplest case is to assume that accumulation where dunes within $ABb_3$ have not been actively re-worked is approximately one dune height (commonly ~15–30 m as reviewed by Bourke et al., 2006). These sub-ice bedforms dominate $ABb_3$ stratigraphy in the ice bridge (Fig. 12B-B'). In the northern part of the transect, layered ice transitions into low albedo, sandy yardangs that lie directly beneath the surface and are being exposed by local ice retreat (Fig. 6A and C). The yardangs transition southward into a large field of buried dunes (Figs. 6C, 12B, 12B-B') that is continuous with those underlying modern dune field S1 (Fig. 9A). The southern end of the transect is characterized by icy yardangs, including those that are being actively exhumed from the layered ice (Fig. 5B and C, Fig. 12B-B'). In the absence of significant re-working, events that generated permafrost surfaces such as those visible beneath dune field S1 and S2 are interpreted to have stabilized dune surfaces, with subsequent dune building events utilizing antecedent topography (Insets 1–3 in Fig. 12B-B').

To the west of the ice bridge, a transect across the windward margin of dune field S2 reveals yet further detail (Fig. 12C). The low surface elevation along the margins of field S2 (Fig. 3B) suggests that locally $ABb_2$ directly overlies the $HBb_r$ surface (Fig. 12C-C'); this is supported by the visible contact between the two units on the southern margin of the dune field (Fig. 11B). Along the northern margin of the field, the $ABb_2$ surface caps and preserves dune topography, indicating sub-$ABb_2$ dunes at this location (Fig. 11C, Inset 2 in Fig. 12C-C'). It is possible that these dunes extend southward and are responsible for the elevation of the pedestal, although without additional evidence, the pedestal is interpreted as icy in nature. Modern perennial layered ice embays the topographic pedestal on which the modern dune field rests; along the field's northern margin, where layered $ABb_3$ ice pinches out on top of $ABb_2$ (Fig. 11C), icy yardangs are being exhumed (Fig. 5B, Inset 1 in Fig. 12C-C'). Within the layered ice deposits

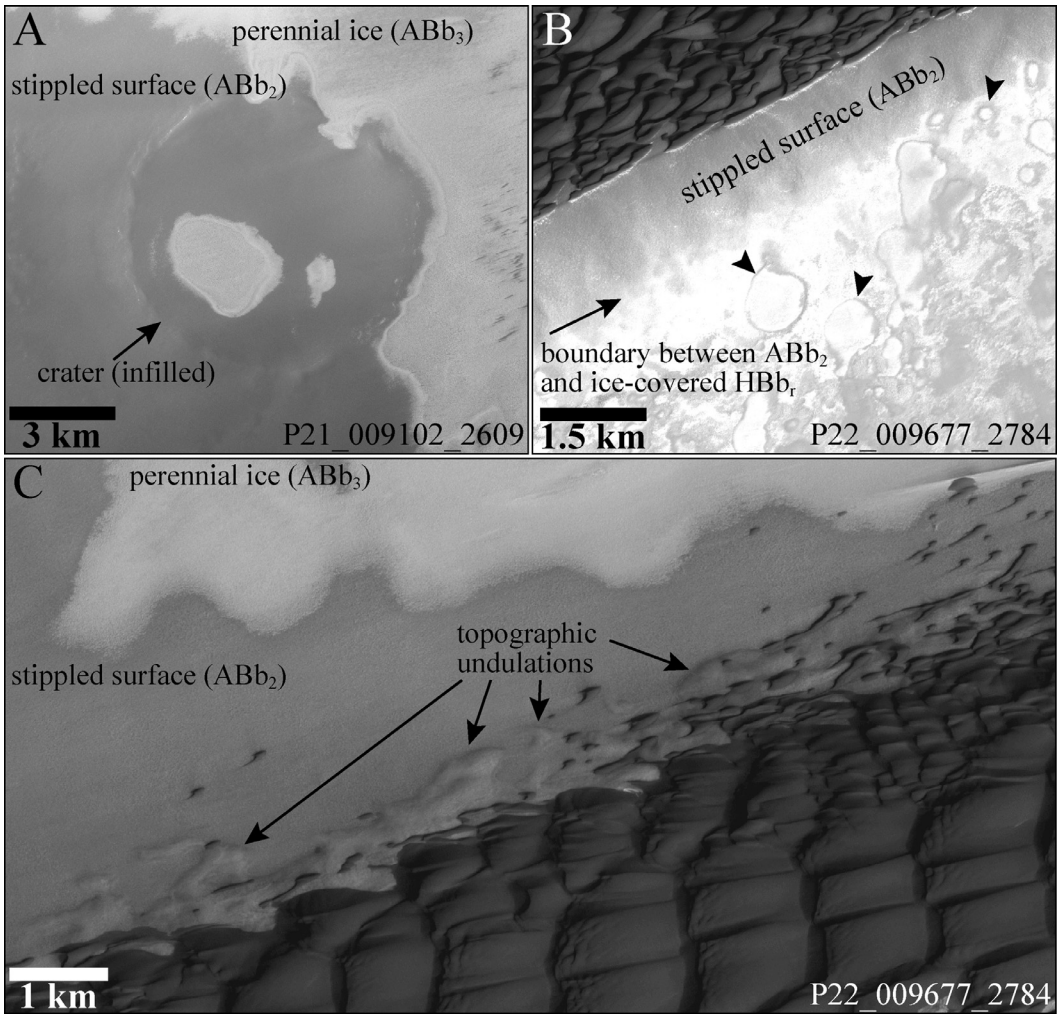


**Fig. 11.** Observations used to differentiate $ABb_2$ from $HBb_r$ and to identify the presence of intervening deposits. (A) An infilled crater blanketed by the stippled surface evidences post-$HBb_r$ deposition. (B) Along the southern margin of field S2, the stippled surface pinches out over the cratered (e.g., black arrows) and eroded $HBb_r$ surface. (C) The northern margin of field S2 forms on $ABb_2$, which exhibits dune-like topographic undulations. Locations are given in Fig. 9B.

along the field's southern margin, $ABb_3$ hosts sand dunes as well as re-worked sand deposits exposed in dune imprints (Fig. 10B, Inset 3 in Fig. 12C-C').

## 5. Controls on deposition, accumulation, and preservation

### *5.1. Boundary condition controls on the depositional environments of Chasma Boreale*

#### *5.1.1. Dune fields*

Chasma Boreale's aeolian system is active as sand sheets, sparse dune cover, and dense dune cover. The dune fields form on ice-free and ice-covered surfaces alike (Fig. 3A), indicating that the boundary conditions controlling the formation and evolution of dune fields are different from those influencing ice deposition and stability. The boundary conditions controlling the occurrence of the dune fields can be hypothesized from the results of geologic mapping coupled with previous work indicating that transport should be dominantly in the down-chasma direction (Spiga et al., 2011). An in-depth analysis of the dune morphologies is beyond the scope of this work, but specific aspects of the dune fields are addressed in Bourke (2006), Mullins et al. (2006), and Schatz et al. (2006).

The northern dune fields (N1-N3, Fig. 1B) each occur immediately downwind of a bedrock outcrop (Fig. 3A). Fields N1 and N2 correspond to discontinuous, linear $ABb_c$ outcrops, whereas field N3 coincides with an $HBb_r$ outcrop (Fig. 9A). The spatial distribution of these fields is most likely a function of the local sediment source areas present upwind. These source areas, particularly the $ABb_c$ outcrops, are postulated to release limited volumes of sediment on a seasonal basis due to mass wasting (c.f., Russell et al., 2008). In such cases, sediment is only seasonally available, and availability of that sediment decays downwind from the outcrop. Some sediment may also be supplied by erosion of the substrate (e.g., Fig. 7B), however, accumulation due to ice stabilization is more prevalent than evidence for substrate erosion (Fig. 9A).

In contrast to the northern dune fields, the southern dune fields (fields S1, S2, Fig. 1B) are larger. Furthermore, the only area of dense dune cover occurs within dune field S2 (Fig. 3A). Neither southern field, however, is associated with a bedrock outcrop (Fig. 9A). Images of the surface showing aeolian scour of the substrate (Fig. 10) argue that the southern dune fields are sourced by deflation of planar, unlithified sand emplaced during prior episodes of aeolian activity. Deflation of these older aeolian sands not only evidences cannibalization of earlier dune accumulations, but also defines a modern sand source that may be exploited at any time during active aeolian abrasion. For both the northern and southern dune fields, the reliance of the dune fields on source area location, geometry, and sediment availability results in a sediment

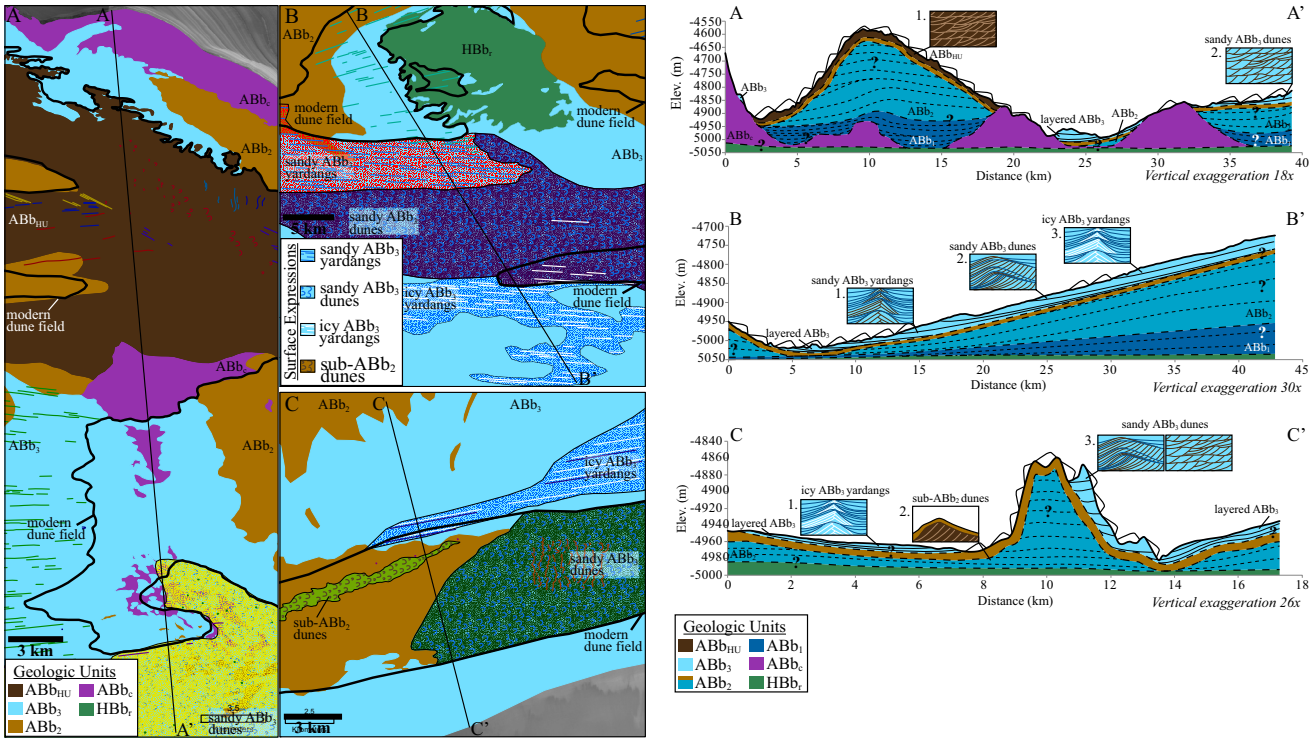


**Fig. 12.** Surface geology and interpreted stratigraphy of Chasma Boreale. Context is given in Fig. 9A. (A) A transect across the head of the reentrant passes between bedrock, layered ice, and modern dune fields (heavy black lines) that are underlain by sand and mixed sand and ice dune accumulations. (B) A transect across the central ice deposits is unique for crossing low albedo yardangs (defrosting linear dunes), transverse bedforms, and icy yardangs. (C) A transect across the windward margin of field S2 transitions from layered ice hosting icy yardangs into modern dune fields. The stippled surface is underlain by dunes. (A-A') Inferred stratigraphy at the head of the reentrant highlights the impact of topographic relief on the mixed sand and ice system. Insets show accumulation of the modern ice-poor and ice-rich dune systems in higher resolution. See Section 5.3. for discussion. Areas where modern dune fields exist on the surface are denoted by trains of bedforms. (B-B') The ice deposits in the center of the reentrant form a smooth ramp increasing in elevation to the south and hosting multiple generations of different bedforms (highlighted in insets). (C-C') The field S2 transect is unique in that it is the only location that dunes are directly capped by the stippled $ABb_2$ surface. Insets show icy yardangs as well as the preserved dunes beneath unit $ABb_2$.

system that responds geomorphically to changes in sediment conditions over spatial scales as short as 10 s of kilometers.

### 5.1.2. Perennial surface ice

In contrast to Planum Boreum, which has accumulated as much as 2 km of layered ice (Phillips et al., 2008) and continues to gain mass through net accumulation of the residual ice cap (Brown et al., 2016), the floor of Chasma Boreale is overall inhospitable to the growth of perennial ice deposits (Fig. 3A). The prevalence of ice-unstable conditions within the reentrant indicates that local boundary conditions prevent ice accumulation. The dominant boundary condition that has been hypothesized to keep the reentrant free of NPLD-scale ice deposits is the topographic funneling of katabatic winds (Holt et al., 2010). As early as end-cavi times, circumpolar katabatic winds and strong katabatic flow off of a bedrock topographic high converged along the axis of proto-Chasma Boreale (Brothers et al., 2015; their Fig. 8). These wind patterns were largely responsible for establishing and enhancing the topography of the reentrant through non-uniform patterns of ice accumulation (Holt et al., 2010).

In the modern system, the effects of katabatic flow from Gemini Lingula and the main lobe of Planum Boreum (Spiga et al., 2011) continue to influence the distribution of perennial surface ice deposits. This occurs both at the reentrant scale, as discussed above, and at the local scale. For example, the ice-free terminus of Hyperborea Lingula is unsheltered from the convergent flow of the plateau's katabatic winds (Spiga et al., 2011). Here, the lack of ice appears to be a function of wind flow coupled with low topographic relief that could otherwise foster ice deposits and perennial ice pack growth (Caine, 1995; Brown and Ward, 1996; Allen, 1998) or promote cold-trapping of water vapor (Svitek and Murray, 1990). Interpreting the outlet of Chasma Boreale as a modern bypass or deflation plain is also supported by the absence of dunes, sand sheets, or remnant dune accumulations (Fig. 3A).

Invoking topographic relief to justify the presence of perennial ice deposits fails along the northern wall of the reentrant and within Boreum Cavus, however. Both of these areas lack perennial surface ice (Fig. 3A), and yet they are the most topographically variable areas of the reentrant (Fig. 3B). Two additional boundary conditions unique to the northern wall may be locally destabilizing perennial surface ice. The first is the reentrant's orientation, which is likely to lead to greater summertime insolation along the more equator-facing wall. Summer insolation is a strong control on the growth of a perennial ice deposit (Huybers and Tziperman, 2008) and may inhibit ice growth under the planet's current moderate obliquity (~25°; Laskar et al., 2002).

The second boundary condition is less apparent but may have the greater effect. Model results for Planum Boreum indicate enhanced warming of the reentrant floor along the northern wall and within Boreum Cavus due to an increase in downward sensible heat flux induced by katabatic winds (Spiga et al., 2011). In these areas, winds deliver as much as 9–12 $W/m^2$ of additional power as sensible heat (Spiga et al., 2011, Fig. 14). This stands in contrast to the southern wall of the reentrant, which receives approximately −1 to 1 $W/m^2$ and therefore undergoes katabatic cooling (Spiga et al., 2011, Fig. 14). The visible distribution of perennial surface ice (Fig. 3A) closely agrees with the hypothesized coupled effect of insolation and warming by katabatic winds and evidences a cryospheric system that varies on horizontal spatial scales as short as those characterizing the aeolian sediment system.

### 5.2. Accumulation

Because boundary conditions controlling the aeolian and cryospheric systems of Chasma Boreale are independent and change over short horizontal distances, the depositional system transitions between aeolian- and ice-dominated surface environments. These result in sand or ice accumulations, respectively (Fig. 9A). The cryosphere-dominated end member of accumulation is NPLD-type layered ice, as found in Chasma Boreale's unit $ABb_3$ (e.g., Figs. 5A and 9A). Layered ice deposits drape underlying topography, infill topographic depressions, and show primary depositional features characteristic of regional sedimentation without a substantial component of traction transport (i.e., bedforms; Murray et al., 1972; Cutts, 1973; Malin and Edgett, 2001; Milkovich and Head, 2005; Fishbaugh et al., 2010; Becerra et al., 2016).

Ice-poor accumulations of cross-stratified dune sand, as characterize unit $ABb_{HU}$ (Figs. 8 and 9A), represent the end member of accumulation controlled by the aeolian system. Accumulation of a body of cross-strata under only the influence of aeolian processes relies upon a positive sand budget in which more sediment enters than exits the system (Kocurek, 1999). Along the northern wall, however, limited sediment sourcing by mass wasting of lithified $ABb_c$ outcrops results in conditions of sediment starvation. Therefore, accumulation of $ABb_{HU}$ is inhibited in this area. Alternatively, the aeolian accumulation may be fixed by sediment cementation, as occurs in terrestrial stabilizing systems such as White Sands, New Mexico (McKee, 1966; Schenk and Fryberger, 1988) or the Bahamas (Caputo, 1995). It is likely that the cross-stratified accumulation of $ABb_{HU}$ relies on induration of dune sediment by pore-filling ice (Schatz et al., 2006; Feldman et al., 2008; Herrmann et al., 2008; Putzig et al., 2013).

Unique to the transitional depositional system of Chasma Boreale is the mixed sand and ice accumulation within unit $ABb_3$. Mixed accumulation ranges from sand-poor and ice-rich, as where few, icy yardangs are separated by NPLD-style layering (Fig. 5B), to sand-rich and ice-poor, such as with the cross-stratified deposits beneath the southern dune fields (Fig. 10) or the interleaving of layered ice with bedforms (Fig. 6C). In the mixed sand and ice accumulation, the stabilizing character of the system is visible as blanketing of dunes by ice (Fig. 6B and C). These deposits define the transitional character of the depositional system. Where active aeolian and surface ice-stable cryospheric systems coincide, relative volumes of ice and sand in the accumulation indicate the balance of processes under local boundary conditions at a given time.

### 5.3. Preservation

Processes of stabilization do not ensure preservation of an accumulation, which is required to form the stratigraphic record. For example, cross-strata accumulated by ice induration may remain at the surface where they are exposed to deflation (Fig. 8), and dune fields buried by ice may defrost (Fig. 6), allowing sediment to remobilize. Furthermore, as seen beneath the southern dune fields, permafrost surfaces and ice layers do not prevent subsequent scour of subsurface sediment deposits (Fig. 10). Although deflation, ice instability, and scour all occur on the modern surface, the presence of an accumulation up to ~800 m thick within Chasma Boreale (Fig. 9B) indicates preservation and the building of a stratigraphic record.

Preservation in Chasma Boreale is accomplished by net accumulation and progressive burial of accumulations (Kocurek and Ewing, 2012). In aeolian systems, progressive burial occurs when local boundary conditions yield a positive sand budget, causing the accumulation surface to rise through time (Kocurek and Havholm, 1993). As discussed above, sediment influx into the reentrant is limited, even within the southern dune fields, which cannibalize the accumulation and therefore contribute little to its rising surface. In the mixed ice-aeolian system, ice may contribute to the rising accumulation surface because surface stabilization retards deflation and re-working, however, aeolian processes may also counteract ice growth by scouring the substrate, potentially limiting frost growth. Additionally, secondary flow over dune topography may locally enhance ice sublimation and help to maintain a low albedo surface that is hostile to ice formation. In the circumstances of competing ice and aeolian processes, an episodic dominance of one process over the other is required to bury the accumulation.

The mantling of dune forms beneath $ABb_2$ (Fig. 11C) is an example of preservation through the burial of an active aeolian system by rapid ice deposition. Current interpretations of the ice-depleted and sediment-rich $ABb_2$ surface suggest the unit was emplaced in an environment dominated by sedimentary processes, yet in sediment starved conditions, yielding a draping sand sheet (Rodriguez et al., 2007). Given the presence of an active dune field, such conditions would have sustained influx of lithic sediment and yielded an increasingly robust aeolian system rather than a draping mantle of sediment. Thus, the deposition of $ABb_2$ must have terminated with rapid ice growth. Rather than forming a thin veneer of ice susceptible to defrosting, as occurs in the modern system (e.g., Fig. 6B and C), ice deposition at the end of $ABb_2$ was sufficient to bury dunes perennially and prevent their exhumation and re-working.

The modern surface expression of the unit, which is desiccated and sediment-rich (Rodriguez et al., 2007), could then have been formed in an extended period of ice instability that resulted in the concentration of lithic sediment at the surface as well as near-surface depletion of ice (Johnson and Lorenz, 2000); such ice-unstable conditions exist currently in parts of the reentrant where the $ABb_2$ surface is exposed (Fig. 9A). The thickness of this armoring sediment lag may be highly variable, but to the northwest of field S2, it is sufficiently thin to express the muted topography of underlying dunes, and thus may be between approximately 10 and 20 m thick (Fig. 12C-C'). This sequence of events leading to the formation of $ABb_2$ has been depicted in Fig. 12A-A'–C-C' as an interval of layered ice capped by a sediment-rich interval that truncates subjacent layers. Analogous processes on Earth are burial by marine sediments during rapid, low-energy marine transgressions (Eschner and Kocurek, 1988) or by lava flow (Mountney et al., 1999; Jerram et al., 2000; Waichel et al., 2008).

## 6. Sequence stratigraphy

Chasma Boreale's stratigraphy illustrates how the depositional system, accumulation, and preservation act to form a polar aeolian sequence. Sequences are used here as initially defined by Mitchum et al. (1977) and applied to aeolian systems by Kocurek and Havholm (1993). Sequences are relatively conformable successions of genetically related strata (stratigraphic packages) bounded by unconformities or their correlative conformable surfaces. Sequence boundaries are typically caused by tectonic, eustatic, or climatic change. Polar aeolian sequences have been interpreted within $ABb_c$. A polar aeolian sequence is defined as a period of aeolian dune construction, which is characterized by sand-rich cross-strata development, followed by a period of surface stabilization, which is characterized by amalgamated permafrost surfaces. The change from active aeolian to ice-stabilized system occurs as a result of basin-scale climatic change (Kocurek et al., 2011).

### 6.1. The Chasma Boreale aeolian sequence

A composite transport-parallel stratigraphic section (Fig. 14A) coupled with a Wheeler diagram (Fig. 14B), or spatio-temporal plot

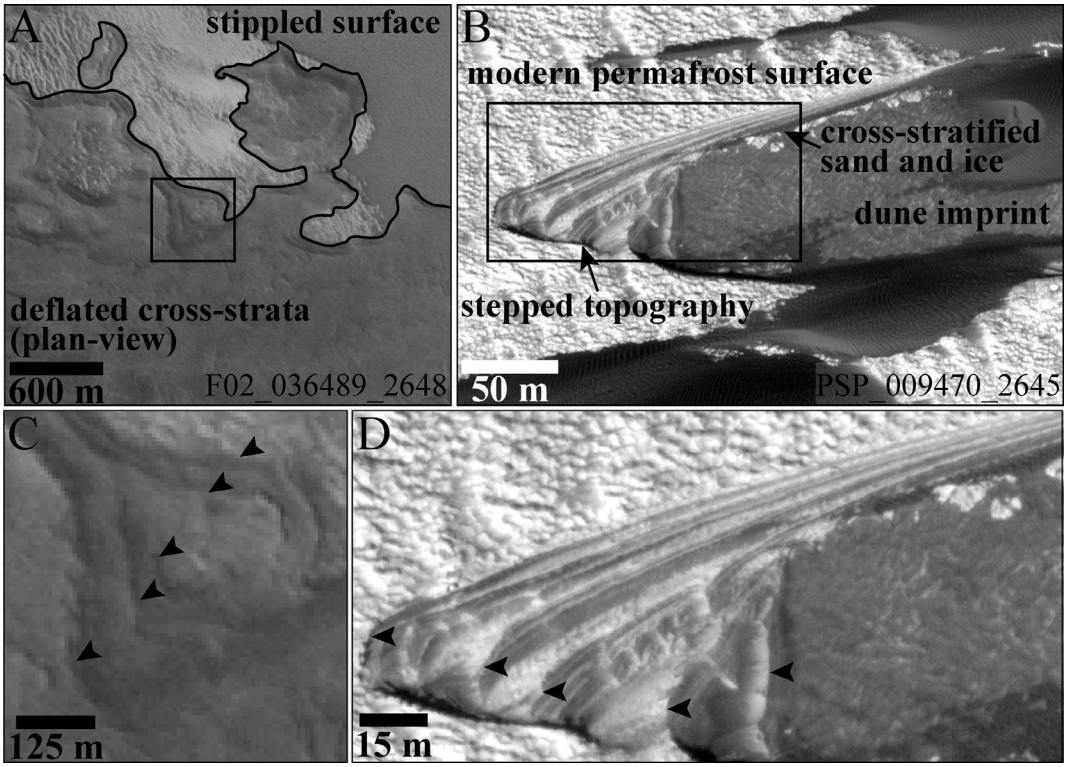


**Fig. 13.** Evidence for high frequency episodes of aeolian construction and deflation in modern dune deposits. (A) The bedded accumulation beneath and extending upwind of field N1 (Fig. 8C) overlies the stippled surface and hosts deflated plan-view cross-strata on its surface. Black box indicates location of (C). (B) A dune imprint beneath field S1 reveals interbedded ice and sand deposits. Black box shows location of (D). Context for this image is shown in Fig. 9B. (C) A zoomed image of the exposed edge of the bedded dune accumulation shows approximately five beds (surfaces denoted by black arrows) each indicating an episode of aeolian construction and deflation. (D) A zoomed image of the dune imprint shows five episodes of permafrost surface formation over aeolian cross-strata.

of preserved accumulations and hiatuses (Wheeler, 1958, 1964), build Chasma Boreale's sequence framework. The $HBb_r$ surface defines the lower bound of the stratigraphic record (Fig. 14A). Accumulation of the $HBb_r$ bench began during the Hesperian, and non-deposition and erosion initiated as early as 3.5 Gyr (Fig. 14B; Tanaka and Fortezzo, 2012). On the terminus of Hyperborea Lingula, these erosional and bypass conditions have persisted to the present (Figs. 9A; 14A, B).

Unit $ABb_c$ deposition initiated some time before 3.6 Myr (Tanaka and Fortezzo, 2012) or 4 Myr (Laskar et al., 2002; Levrard et al., 2007), but after a period of hiatus during which any stratigraphic record representing the time between units $HBb_r$ and $ABb_c$ was removed (Fig. 14B). While erosional outcrops of $ABb_c$ in Chasma Boreale's wall indicate deposition within the reentrant was more extensive than what is mapped, evidence for a prior, larger extent of $ABb_c$ does not remain on the reentrant floor. Although elsewhere on the plateau, $ABb_c$ accumulations transition gradationally into the NPLD (Tanaka et al., 2008; Kocurek et al., 2011; Brothers et al., 2017), within the reentrant the surface of $ABb_c$ is erosional (Fig. 14A) and succeeded by a second, shorter hiatus (Fig. 14B).

The oldest preserved ice accumulations within the reentrant are as old as unit $ABb_1$ or as young as unit $ABb_2$ and are hypothesized based on accumulation thickness, although their precise distribution is uncertain (Fig. 14B). Based upon crater dating by Tanaka and Fortezzo (2012), the oldest layered ice deposits are dated as beginning at 3.6 Myr (Fig. 14B); although older estimates have been made for NPLD initiation (~ 4 Myr; Levrard et al., 2007), the younger age better reflects that these ice deposits uncomfortably overlie $ABb_c$, which was contemporary with the oldest NPLD (Brothers et al., 2017). These early ice deposits coexisted or interbedded with at least one active aeolian field (Figs. 12; 14A, B). As in the modern system, additional fields most likely existed up-chasma in areas of greater net accumulation, which are also proximal to eroding cavi unit outcrops and potential sediment sources (e.g., below dune fields N1 and S1; Fig. 9B). Aeolian activity was halted by rapid ice growth within unit $ABb_2$, which was followed by reentrant-wide deflation associated with the unconformable $ABb_2$ sequence surface. The development of unit $ABb_2$, which preserves dune topography and remains exposed to deflation in places marks the end of an aeolian sequence (Fig. 14).

The modern aeolian sequence benefits from an increase in vertical and lateral resolution (Fig. 14C), providing a clear record of early sequence development. The current sequence initiated with development of an active depositional system that laterally transitions between the ice-poor cross-strata of $ABb_{HU}$, mixed layered ice and cross-strata of $ABb_3$, and $ABb_3$ layered ice. Accumulations are separated by bypass and deflation surfaces where the $ABb_2$ sequence surface remains exposed (Fig. 14B). The aeolian record of accumulation and deflation in unit $ABb_{HU}$ (Fig. 13A, C) and comparable mixed accumulation intervals (Fig. 13B, D) are indicative of higher frequency episodes of aeolian activity punctuated by periods of either stabilization by permafrost surfaces, where surface ice is stable, or by deflation.

### 6.2. Defining a transitional aeolian sequence

The Chasma Boreale depositional system is best used to understand the dynamics of an aeolian-ice transitional system, including how competing and complementary aeolian and cryospheric processes build an accumulation, what the architecture of that

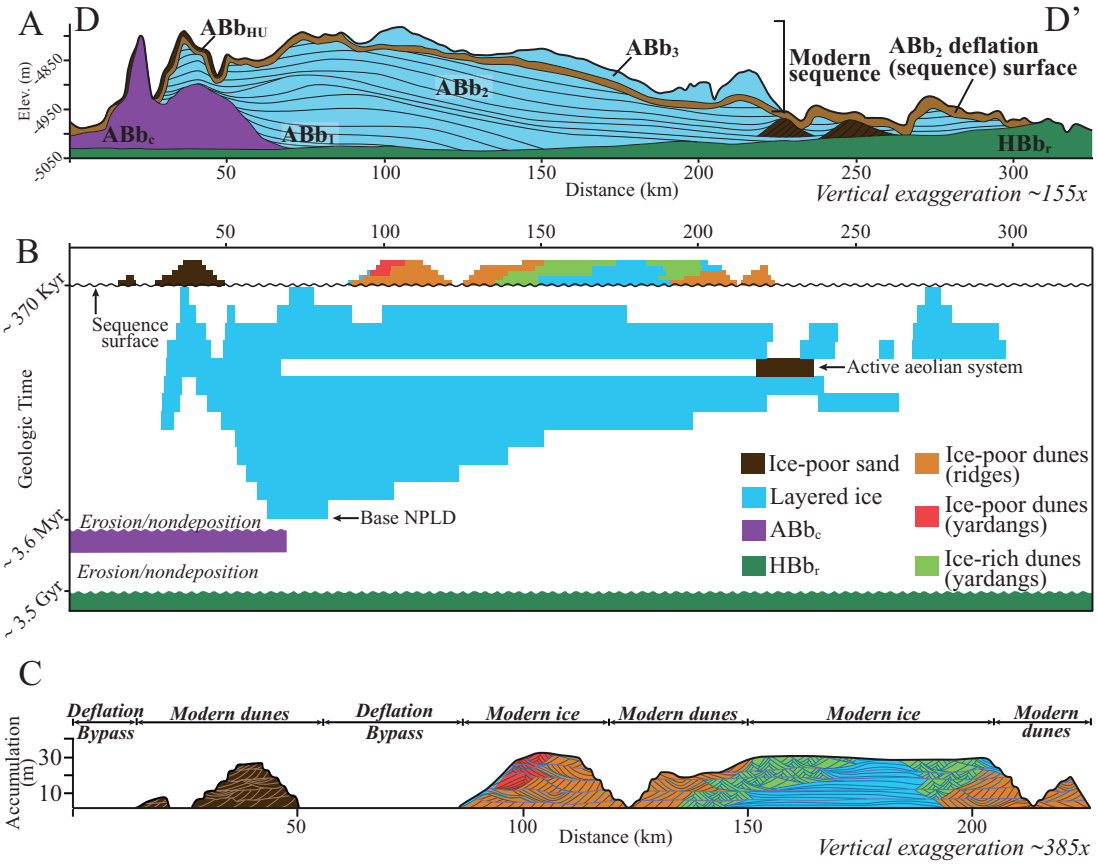


**Fig. 14.** Interpreted sequence stratigraphy and chronostratigraphy of the Chasma Boreale transitional depositional system. (A) A stratigraphic section approximately parallel to the reentrant passes through the different modern depositional environments (transect D-D' in Fig. 9A). An older polar aeolian sequence underlies the deflation surface of $ABb_2$, which is an aeolian sequence boundary. Renewed accumulation in $ABb_{HU}$ and $ABb_3$ represents the beginning of a new (modern) sequence. (B) Inferred chronostratigraphy of Chasma Boreale portrayed as a Wheeler Diagram (plot representing accumulation and erosion as a function of time and place). Note that the vertical portrayal of geologic time is nonlinear. (C) Accumulation in Chasma Boreale since development of the $ABb_2$ surface, flattened on the $ABb_2$ surface. Approximately five episodes of aeolian construction and deflation are present within the accumulations of $ABb_{HU}$ and $ABb_3$. The estimation of vertical scale of post-$ABb_2$ accumulation is discussed in the text.

accumulation looks like, and how the accumulation becomes preserved. Upward translation of these principles yields a succession of stratigraphic sequences in which each stratigraphic package is terminated by a preserving interval of ice. In this way, the transitional aeolian sequence of Chasma Boreale agrees with previous definitions of Martian polar aeolian sequences applied to the cavi unit (Kocurek et al., 2011). The primary difference is that a transitional sequence incorporates the architectures of co-active aeolian and cryospheric systems within the same accumulation.

The coincidence of complementary and competing aeolian and ice processes within a transitional depositional system highlights a dynamic of the polar sedimentary system hitherto unaddressed. Prior studies have focused on either aeolian depositional environments, such as prevail in the polar erg of Olympia Undae (Tsoar et al., 1979; Feldman et al., 2008; Ewing et al., 2010), or layered ice environments, as exist on top of the plateau (Fishbaugh et al., 2010; Becerra et al., 2016). Within Chasma Boreale, these environments occur together as a function of local boundary conditions, evidencing how under a single regional climate, sequence architecture can transition laterally between dune fields, ice deposits, and bypass or deflation surfaces. As evidenced by the variable accumulation on the floor of Chasma Boreale, volumes of accumulated material also change drastically within a sequence. As a result, episodes of aeolian or ice activity may be better recorded in certain parts of the system than others, and sequence boundaries may pass laterally into inactive areas, thus becoming indistinguishable.

The spatial heterogeneities that characterize the transitional depositional system and resultant sequence architecture bear implications for interpreting controls on sequence development. Local boundary conditions play a dominant role in sequence architecture. This is evidenced by the short lateral transitions between ice-dominated and sand-dominated environments. High frequency fluctuations between sand and ice co-activity capped by aeolian deflation and surface stabilization are expressed as a function of local boundary conditions as well. This is seen in the difference between $ABb_{HU}$ and $ABb_3$ (Fig. 13) and makes correlating discrete episodes within a single depositional system difficult. These fluctuations may be unique to their depositional system and therefore driven by autogenic dynamics, or they may be controlled by an allogenic forcing coupled nonlinearly with the strong influence of local boundary conditions.

Sequence-capping ice deposits are the feature least susceptible, although not immune to, local boundary conditions. While within Chasma Boreale a reentrant-wide layered ice deposit must have been present to shut down the existing aeolian system, the thickness of that ice accumulation is most likely variable. This is deduced from the inference of a mixed system preceding ice deposition. Layered ice deposits would have initiated in surface ice-stable areas of the reentrant and transgressed the system from those areas as ice became increasingly more stable. Concomitantly, aeolian activity would have waned without ceasing as ice covered

potential sediment source areas. The result, however, is a sequence in which layered ice is present from base to top at one location, while in another, layered ice may initiate abruptly on top of an aeolian complex, giving the appearance of an instant environmental change.

### 6.3. Orbital forcing of sequences

Interpreting basin-scale climate change from polar aeolian sequences contributes to efforts to relate Planum Boreum's stratigraphy to orbital forcing on climate. The sequence stratigraphy of Chasma Boreale's accumulation is ill-suited to this because stratigraphy preceding the $ABb_2$ sequence surface is uncertain, and multiple older sequences may exist. Relating events of the modern, post-$ABb_2$ sequence with contemporary events occurring on Planum Boreum, however, is reasonable. The $ABb_2/ABb_3$ sequence transition that occurs in visible imagery (Tanaka et al., 2008; Tanaka and Fortezzo, 2012) has been anecdotally related to a widespread angular unconformity in the subsurface of the NPLD (Smith et al., 2016). This, in turn, indicates a period of polar ice instability, such as occurs during Martian ice ages when ice migrates toward the mid-latitudes (Head et al., 2003). The most recent ice age is modeled to have occurred at ~370 Kyr (Head et al., 2003).

It is tempting to relate the higher frequency cycles within the $ABb_3$ transitional sequence to allogenic forcing by orbital climate change. On the plateau, ~6–8 visible ice layers constitute $ABb_3$ (Tanaka and Fortezzo, 2012). This corresponds with a similar number of reflections in the postulated radar-equivalent unit (Smith et al., 2016). These, in turn, agree with the number of high frequency aeolian episodes recorded in the Chasma Boreale transitional system (Fig. 13). Using 370 Kyr for the sequence boundary, six high frequency episodes would correspond to approximately three 120 Kyr insolation cycles (Levrard et al., 2007), or an aeolian-to-ice transition each half insolation cycle.

While tempting, an approach to dating layer formation using high frequency episodes within the most recent sequence is flawed in that it yields a severe mismatch between the number of layers and the number of insolation cycles that have occurred since the increase in polar ice stability at ~4 Myr (Levrard et al., 2007). This is supported by findings reported by Brothers et al. (2017) and which offer an alternative, more robust interpretation of allogenic forcing of polar sequences. At present, these high frequency episodes are more prudently regarded as driven by an autogenic dynamic that is most clearly expressed in the transition between aeolian and cryosphere processes, but that is not yet understood.

## 7. Conclusions

The Chasma Boreale depositional system is unique for exhibiting characteristics of both the dominantly aeolian environments around Planum Boreum as well as those of the layered ice deposits on the plateau. The coexistence of these depositional environments results in a transitional system that shows the competing and complementary dynamics of aeolian and ice processes. These are strongly governed by local boundary conditions, resulting in a spatially heterogeneous depositional system. Boundary conditions change through time, resulting in laterally shifting aeolian and cryospheric environments. Regional and possibly global changes in climate overprint local boundary conditions and have resulted in the development of at least one aeolian sequence, characterized by a period of relatively rapid ice growth and capped by a deflation surface, on the reentrant floor.

The Chasma Boreale sequence demonstrates how transitional system sequences differ from previously identified cavi unit sequences. Within the transitional sequence, aeolian and ice systems are active concurrently within a single depositional environment, and periods of surface stabilization and ice transgression are marked by thick deposits of topography-preserving layered ice instead of thin, amalgamated permafrost surfaces. The presence of cavi unit sequences transitioning gradationally from aeolian to ice environments both elsewhere on Planum Boreum and within the reentrant (Brothers et al., 2017) suggests that the Chasma Boreale depositional system and accumulation provide elegant process and stratigraphic analogs for sections of the cavi unit that transition gradationally into the NPLD.

## Acknowledgments

The identification of time series CTX images of the appropriate season benefited from the help of T.C. Brothers. The initial work was greatly improved by reviews from and discussion with S. Byrne, C. Hern, J.W. Holt, and D. Mohrig. Two anonymous reviewers also greatly helped in producing the final manuscript. This research has been supported by NASA's Mars Data Analysis Program grant number NNX15AM52G and the University of Texas at Austin, Jackson School of Geosciences.

## References

Allen, T.R., 1998. Topographic context of glaciers and perennial snowfields, Glacier National Park, Montana. Geomorphology 21, 207–216.
Becerra, P., Byrne, S., Sori, M.M., Sutton, S., Herkenhoff, K.E., 2016. Stratigraphy of the north polar layered deposits of Mars from high-resolution topography. J. Gephys. Res.: Planets 121, 1445–1471.
Benito, G., Mediavilla, F., Fernandez, M., Marquez, A., Martinez, J., Anguita, F., 1997. Chasma Boreale, Mars: a sapping and outflow channel with a tectono-thermal origin. Icaurs 129, 528–538.
Bourke, M.C. (2006) A New Model for Linear Dune Formation: Merged Barchan Convoys on Mars. *Lunar and Planetary Science XXXVII*, Abstract #2432.
Bourke, M.C., Balme, M., Beyer, R.A., Williams, K.K., Zimbelman, J., 2006. A comparison of methods used to estimate the height of sand dunes on Mars. Geomorphology 81, 440–452.
Brothers, S.C., Kocurek, G., Holt, J.W., 2017. Sequence architecture of the cavi unit, Chasma Boreale, Mars. Icarus Submitted for publication.
Brothers, T.C., Holt, J.W., Spiga, A., 2015. Planum Boreum basal unit topography, Mars: irregularities and insights from SHARAD. J. Geophys. Res.: Planets 120, 1357–1375.
Brown, I., Ward, R., 1996. The influence of topography on snowpatch distribution in southern iceland: a new hypothesis for glacier formation? Geogr. Ann. Ser. A Phys. Geogr. 78 (4), 197–207.
Brown, A.J., Calvin, W.M., Becerra, P., Byrne, S., 2016. Martian north polar cap summer water cycle. Icarus 277, 401–415.
Byrne, S., 2009. The polar deposits of Mars. Annu. Rev. Earth Planet. Sci. 37, 535–560.
Byrne, S., Murray, B.C., 2002. North polar stratigraphy and the paleo-erg of Mars. J. Geophys. Res. 107 (E6, 5044), 13.
Caine, N., 1995. Snowpack influences on geomorphic processes in Green Lakes Valley, Colorado front range. Geogr. J. 161 (1), 55–68.
Caputo, M.V., 1995. Sedimentary architecture of Pleistocene eolian calcarenites, San Salvador Island, Bahamas. Geol. Soc. Am. 300, 63–76 Special Papers.
Cutts, J.A., 1973. Nature and origin of layered deposits of the Martian polar regions. J. Geophys. Res. 78 (20), 4231–4249.
Edwards, C.S., Nowicki, K.J., Christensen, P.R., Hill, J., Gorelick, N., Murray, K., 2011. Mosaicking of global planetary image datasets: 1. Techniques and data processing for Thermal Emission Imaging System (THEMIS) multi-spectral data. J. Geophys. Res.: Planets 116 (E10008), 21.
Eschner, T.B., Kocurek, G., 1988. Origins of relief along contacts between eolian sandstones and overlying marine strata. Am. Assoc. Pet. Geol. Bull. 72 (8), 932–943.
Ewing, R.C., Peyret, A.-P.B., Kocurek, G., Bourke, M., 2010. Dune field pattern formation and recent transporting winds in the Olympia Undae Dune Field, north polar region of Mars. J. Geophys. Res. 115 (E08005), 25.
Feldman, W.C., Bourke, M.C., Elphic, R.C., Maurice, S., Bandfield, J., Prettyman, T.H., Diez, B., Lawrence, D.J., 2008. Hydrogen content of sand dunes within Olympia Undae. Icarus 196 (2), 422–432.
Fishbaugh, K.E., Head, J.W., 2002. Chasma Boreale, Mars: topographic characterization from Mars orbiter laster altimeter data and implications for mechanisms of formation. J. Geophys. Res. 107 (E3), 23.
Fishbaugh, K.E., Head, J.W., 2005. Origin and characteristics of the Mars north polar basal unit and implications for polar geologic history. Icarus 174, 444–474.
Fishbaugh, K.E., Byrne, S., Herkenhoff, K.E., Kirk, R.L., Fortezzo, C., Russell, P.S., McEwen, A., 2010. Evaluating the meaning of "layer" in the Martian north polar layered deposits and the impact on the climate connection. Icarus 205, 269–282.
Grima, C., Kofman, W., Mouginot, J., Phillips, R.J., Herique, A., Biccari, D., Seu, R., Cutigni, M., 2009. North polar deposits of Mars: extreme purity of the water ice. Geophys. Res. Lett. 36 (L03203), 4.

Hayward, R.K., Mullins, K.F., Fenton, L.K., Hare, T.M., Titus, T.N., Bourke, M.C., Colaprete, A., Christensen, P.R., 2007. Mars global digital dune database and initial science results. J. Geophys. Res. 112 (E11007), 17.
Head, J.W., Mustard, J.F., Kreslavsky, M.A., Milliken, R.E., Marchant, D.R., 2003. Recent ice ages on Mars. Nature 426, 797–802.
Herkenhoff, K.E., Byrne, S., Russell, P.S., Fishbaugh, K.E., McEwen, A.S., 2007. Meter-scale morphology of the north polar region of Mars. Science 317, 1711–1715.
Herrmann, H.J., Duran, O., Parteli, E.J.R., Schatz, V., 2008. Vegetation and induration as sand dunes stabilizers. J. Coast. Res. 24 (6), 1357–1368.
Holt, J.W., Fishbaugh, K.E., Byrne, S., Christian, S., Tanaka, K., Russell, P.S., Herkenhoff, K.E., Safaeinili, A., Putzig, N.E., Phillips, R.J., 2010. The construction of Chasma Boreale on Mars. Nature 465, 446–449.
Howard, A.D., 2000. The role of eolian processes in forming surface features of the Martian polar layered deposits. Icarus 144, 267–288.
Huybers, P., Tziperman, E., 2008. Integrated summer insolation forcing and 40,000-year glacial cycles: the perspective from an ice-sheet/energy-balance model. Paleoceanography 23 (PA1208), 18.
Hvidberg, C.S., Fishbaugh, K.E., Winstrup, M., Svensson, A., Byrne, S., Herkenhoff, K.E., 2012. Reading the climate record of the Martian polar layered deposits. Icarus 221 (1), 405–419.
Jerram, D.A., Mountney, N.P., Howell, J.A., Long, D., Stollhofen, H., 2000. Death of a sand sea: an active aeolian erg systematically buried by the Etendeka flood basalts of NW Namibia. J. Geol. Soc. Lond. 157, 513–516.
Johnson, J.B., Lorenz, R.D., 2000. Thermophysical properties of Alaskan loess: an analog material for the Martian polar layered terrain? Geophys. Res. Lett. 27 (17), 2769–2772.
Kocurek, G., 1999. The aeolian rock record (yes, Virginia, it exists, but it really is rather special to create one). In: Goudie, A.S., Livingstone, I., Stokes, S. (Eds.), Aeolian Environments, Sediments, and Landforms. John Wiley & Sons, Ltd., pp. 239–259.
Kocurek, G., Ewing, R.C., 2012. Source-to-sink: an Earth/Mars comparison of boundary conditions for eolian dune systems. Sediment. Geol. Mars 102, 151–168 SEPM Special Publication.
Kocurek, G., Havholm, K.G., 1993. Eolian sequence stratigraphy – a conceptual framework. In: Weimer, P., Posamentier, H. (Eds.). In: Siliciclastic Sequence Stratigraphy, 58. American Association Petroleum Geologists Memoir, pp. 393–409.
Kocurek, G., Ewing, R.C., Christian, S., Holt, J.W., 2011. Sequence stratigraphy of the Planum Boreum Cavi unit, north polar region of Mars. In: Proceedings of the 5th Mars Polar Science Conference Abtract #6020.
Laskar, J., Levrard, B., Mustard, J.F., 2002. Orbital forcing of the martian polar layered deposits. Nature 419, 375–377.
Laskar, J., Correia, A.C.M., Gastineau, M., Joutel, F., Levrard, B., Robutel, P., 2004. Long term evolution and chaotic diffusion of the insolation quantities of Mars. Icarus 170 (2), 343–364.
Levrard, B., Forget, F., Montmessan, F., Laskar, J., 2007. Recent formation and evolution of northern Martian polar layered deposits as inferred from a global climate model. J. Geophys. Res. 112 (E06012), 18.
Malin, M.C., Edgett, K.S., 2001. Mars global surveyor Mars orbiter camera: interplanetary cruise through primary mission. J. Geophys. Res. 106 (E10), 23429–23570.
Malin, M.C., Bell, J.F., Cantor, B.A., Caplinger, M.A., Calvin, W.M., Clancy, R.T., Edgett, K.S., Edwards, L., Haberle, R.M., James, P.B., Lee, S.W., Ravine, M.A., Thomas, P.C., Wolff, M.J., 2007. Context camera investigation on board the Mars reconnaissance orbiter. J. Geophys. Res. 112 (E05S04), 25.
McEwen, A.S., Eliason, E.M., Bergstrom, J.W., Bridges, N.T., Hansen, C.J., Delamere, W.A., Grant, J.A., Gulick, V.C., Herkenhoff, K.E., Keszthelyi, L., Kirk, R.L., Mellon, M.T., Squyres, S.W., Thomas, N., Weitz, C.M., 2007. Mars reconnaissance Orbiter's High Resolution Imaging Science Experiment (HiRISE). J. Geophys. Res. 112 (E05S02), 40.
McKee, E.D., 1966. Structures of dunes at White Sands National Monument, New Mexico (and a comparison with structures of dunes from other selected areas). Sedimentology 7, 1–69.
Milkovich, S.M., Head, J.W., 2005. North polar cap of Mars: polar layered deposit characterization and identification of a fundamental climate signal. J. Geophys. Res. 110 (E01005), 21.
Mitchum, R.M., Vail, P.R., Thompson, S., 1977. Seismic stratigraphy and global changes of sea level, part 2: the depositional sequence as a basic unit for stratigraphic analysis. In: Payton, C.E. (Ed.), Seismic Stratigraphy – Applications to Hydrocarbon Exploration. The American Association of Petroleum Geologists, Tulsa, Oklahoma, p. 516.
Mountney, N., Howell, J., Flint, S., Jerram, D., 1999. Relating eolian bounding-surface geometries to the bed forms that generated them: Etjo Formation, Cretaceous, Namibia. Geology 27 (2), 159–162.
Mullins, K.F., Hayward, R., Tanaka, K.L., 2006. Dune forms and ages and associated oblate depressions in the Chasma Boreale region of Planum Boreum, Mars. In: Proceedings of the 37th Lunar and Planetary Science Conference Abstract #1998.
Murray, B.C., Soderblom, L.A., Cutts, J.A., Sharp, R.P., Milton, D.J., Leighton, R.B., 1972. Geological framework of the south polar region of Mars. Icarus 17, 328–345.
Nunes, D.C., Phillips, R.J., 2006. Radar subsurface mapping of the polar layered deposits on Mars. J. Geophys. Res. 111 (E06S21), 16.
Parteli, E.J.R., Duran, O., Bourke, M.C., Tsoar, H., Poschel, T., Herrmann, H., 2014. Origins of Barchan dune asymmetry: insights from numerical simulations. Aeolian Res. 12, 121–133.
Phillips, R.J.26 colleagues, 2008. Mars north polar deposits: stratigraphy, age and geodynamical response. Science 320, 1182–1185.
Putzig, N.E., Phillips, R.J., Campbell, B.A., Holt, J.W., Plaut, J.J., Carter, L.M., Egan, A.F., Bernardini, F., Safaeinili, Seu, R., 2009. Subsurface structure of Planum Boreum from Mars reconnaissance orbiter shallow radar soundings. Icarus 204, 443–457.
Putzig, N.E., Mellon, M.T., Herkenhoff, K.E., Phillips, R.J., Davis, B.J., Ewer, K.J., Bowers, L.M., 2013. Thermal behavior and ice-table depth within the north polar erg of Mars. Icarus 230, 64–76.
Rodriguez, J.A.P., Tanaka, K.L., Langevin, Y., Bourke, M., Kargel, J., Christensen, P., Sasaki, S., 2007. Recent aeolian erosion and deposition in the north polar plateau of Mars. Mars: Int. J. Mars Sci. Explor. 3, 29–41.
Russell, P., Thomas, N., Byrne, S., Herkenhoff, K., Fishbaugh, K., Bridges, N., Okubo, C., Milazzo, M., Daubar, I., Hansen, C., McEwen, A., 2008. Seasonally active frost–dust avalanches on a north polar scarp of Mars captured by HiRISE. Geophys. Res. Lett. 35 (L23204), 5.
Schenk, C.S., Fryberger, S.G., 1988. Early diagenesis of eolian dune and interdune sands at White Sands, New Mexico. Sediment. Geol. 55, 109–120.
Schatz, V., Tsoar, H., Edgett, K.S., Parteli, E.J.R., Herrmann, H.J., 2006. Evidence for indurated sand dunes in the Martian north polar region. J. Geophys. Res. 111 (E04006), 14.
Smith, D.E., Zuber, M.T., Frey, H.V., Garvin, J.B., Head, J.W., Muhleman, D.O., Pettengill, G.H., Phillips, R.J., Solomon, S.C., Zwally, H.J., Banerdt, W.B., Duxbury, T.C., Golombek, M.P., Lemoine, F.G., Neumann, G.A., Rowlands, D.D., Aharonson, O., Ford, P.G., Ivanov, A.B., Johnson, C.L., McGovern, P.J., Abshire, J.B., Afzal, R.S., Sun, X., 2001. Mars orbiter laser altimeter: experiment summary after the first year of global mapping of Mars. J. Geophys. Res. 106 (E10), 23689–23722.
Smith, D., Neumann, G., Arvidson, R.E., Guiness, E.A., Slavney, S. (2003) Mars Global Surveyor Laser Altimeter Mission Experiment Gridded Data Record. NASA Planetary Data System. MGS-M-MOLA-5-MEGDR-L3-V1.0.
Smith, I.B., Putzig, N.E., Holt, J.W., Phillips, R.J., 2016. An ice age recorded in the polar deposits of Mars. Science 352, 1075–1078.
Spiga, A., Forget, F., Madeleine, J.-B., Montabone, L., Lewis, S.R., Millour, E., 2011. The impact of Martian mesoscale winds on surface temperature and on the determination of thermal inertia. Icarus 212, 504–519.
Svitek, T., Murray, B., 1990. Winter frost at viking lander 2 site. J. Geophys. Res. 95 (B2), 1495–1510.
Tanaka, K.L., Rodriguez, J.A.P., Skinner, J.A., Bourke, M.C., Fortezzo, C.M., Herkenhoff, K.E., Kolb, E.J., Okubo, C.H., 2008. North polar region of Mars: advances in stratigraphy, structure, and erosional modification. Icarus 196, 318–358.
Tanaka, K.L., Fortezzo, C.M. Geologic Map of the North Polar Region of Mars: U.S Geological Survey Scientific Investigations Map 3177, scale 1:2,000,000.
Toon, O.B., Pollack, J.B., Ward, W., Burns, J.A., Bilksi, K., 1980. The astronomical theory of climate change on Mars. Icarus 44, 552–607.
Tsoar, H., Greeley, R., Peterfreund, A.R., 1979. Mars: the North Polar Sand Sea and related wind patterns. J. Geophys. Res. 84 (B14), 8167–8180.
Waichel, B.L., Scherer, C.M.S., Frank, H.T., 2008. Basaltic lava flows covering active aeolian dunes in the Parana Basin in southern Brazil: features and emplacement aspects. J. Volcanol. Geotherm. Res. 171, 59–72.
Warner, N.H., Farmer, J.D., 2008. Importance of aeolian processes in the origin of the north polar Chasmata, Mars. Icarus 196, 368–384.
Wheeler, H.E., 1958. Time-stratigraphy. Bull. Am. Assoc. Pet. Geol. 42 (5), 1047–1063.
Wheeler, H.E., 1964. Baselevel, lithosphere surface, and time-stratigraphy. Geol. Soc. Am. Bull. 75, 599–610.